J. Indian Inst. Sci.
A Multidisciplinary Reviews Journal
ISSN: 0970-4140 Coden-JIISAD

REVIEW ARTICLE

Magnesium Silicate Bioceramics for Bone Regeneration: A Review

K. Bavya Devi[1], *Samit Kumar Nandi*[2*] *and Mangal Roy*[1*]

Abstract | With the increase in need of ideal bone graft materials, magnesium silicate has been explored as resorbable bioceramics. Calcium phosphate-based bioceramics are well studied and being implemented for several orthopaedic applications as they mimic the chemistry of the natural bone. Although extensively used, these materials do not satisfy all the essential requirements of an ideal temporary bone replacement material. Materials, such as tricalcium phosphate (TCP) and hydroxyapatite (HA), have low solubility and often the resorption rate is quite slow when implanted in vivo. The research on magnesium silicate for bone regenerative application is quite relatively young and a new area compared to traditional calcium phosphate-based materials. Although limited research findings have been reported, it is believed that magnesium silicate-based bioceramics may be an alternative to calcium phosphate for bone tissue engineering applications. Thus in this review, we have highlighted the importance of magnesium silicate bioceramics and compared with existing calcium phosphate ceramics. We have also analysed the future directions and the need for clinical implementations.

1 Clinical need for degradable bioceramics

The demand for new bone substitutes with the physical, mechanical and biological properties matching that of bone is of great importance. Starting from the early 1960s, a wide variety of biomaterials such as metals[1], polymers[2], ceramics[3, 4] and composites[5] have been used in the biomedical field. Among all, ceramics are increasingly used to treat bone defects, small fractures of tibia, dental, maxillofacial reconstruction and spinal discs[6]. Bioceramics, particularly calcium phosphate-based ceramics, namely hydroxyapatite ($Ca_{10}(PO_4)_6(OH)_2$) (HA), dicalcium phosphate dihydrate ($CaHPO_4{\cdot}2H_2O$) (DCPD) and tricalcium phosphate ($Ca_3(PO_4)_2$) (TCP), have been widely used as bone replacement substituents because of their similarity in chemical composition to the natural bone, good biocompatibility and osseointegration. Limited solubility of HA and TCP also raises a question on the true nature of the degradable bioceramics[7–9]. Keeping the degradability in mind, newer bioceramics have been developed for lower life span in the human body with similar biocompatibility and bone regeneration ability.

The chemical composition of bioceramics is an important parameter that governs their degradability, biocompatibility and bioactivity when implanted in vivo. Further, it has been reported that the dissoluted or degraded ions, from the implanted material, stimulate the surrounding environment for new bone formation[10]. Recently research efforts have focussed on biodegradable implant materials that degrades completely in the body leaving no toxic products and, hence, no secondary surgery is needed for implant removal[11]. For this purpose, the implant materials are made with an interconnected porous structure which allows the diffusion of essential nutrients, and cell proliferation which allows the bone tissue to grow forming a strong bond with the implant material[12–14]. Recently, magnesium-based silicate ceramics, forsterite (Mg_2SiO_4) (MgS), a young field of research, have been investigated because of the beneficial role of Mg and Si ions for bone

[1] *Department of Metallurgical and Materials Engineering, Indian Institute of Technology, Kharagpur, Kharagpur 721302, India.*
[2] *Department of Veterinary Surgery and Radiology, West Bengal University of Animal and Fishery Sciences, Kolkata 700037, India.*
**samitnandi1967@gmail.com*
mroy@metal.iitkgp.ac.in

regeneration[15, 16]. The enhanced degradation rate, good biocompatibility and solubility of forsterite gained significant interest in the field of bone tissue engineering[10, 17]. Research findings of Naghiu et al. proved that the dissoluted products of forsterite improved the osteoblast proliferation of U20S-type cells without cytotoxic effect[18]. Similar studies of Ni et al. also showed the well-covered proliferated cells on the surface of the forsterite ceramics, confirming that the degraded ions from forsterite bioceramics increased the proliferation rate than control samples over 7 days[19].

This review focuses on the growth and achievements of forsterite bioceramics for bone regeneration applications till date. We first discussed the importance of Mg and Si ions in bone regeneration metabolism. Further, we moved to the synthesis methods using various techniques followed by complete in vitro biological behaviour and in vivo biocompatibility of the forsterite ceramics. Finally, we conclude that the forsterite bioceramics are suitable compared with the calcium phosphate-based ceramics in the future directions and the clinical implementations of it.

2 Significance of Mg and Si ions in bone metabolism

In addition to calcium (Ca), magnesium (Mg) is also an essential element in the human body as it plays an important key role in bone metabolism, DNA stabilization, and skeletal development[20, 21]. Research findings have showed that magnesium increases the proliferation and stimulation of osteoblastic cell growth[22–24]. The released Mg ions from porous magnesium scaffold showed good cytocompatibility and increased the ALP activity and expression of osteogenic differentiation. Further, the in vivo studies in rabbit model reported mature bone regeneration at the bone–implant site[25]. The deficiency of Mg leads to loss in bone mass, decreased bone growth, increased skeletal fragility and a risk factor for osteoporosis[26–29].

Similarly, silicon (Si), an important element in the metabolic processes, helps in the development and calcification of bone tissue[30]. Studies have showed that the trace amount of Si helps in bone repair, regulates the production of collagen type 1, and plays an essential role as a cross-linking agent in the connective tissue[31]. It also improves bioactivity, promotes osteoblast differentiation and mineralization of bone[32]. Substitution of 0.8% wt of Si in hydroxyapatite enhanced the metabolic activity, stimulated the expression of type I collagen and increased the proliferation of human osteosarcoma cells (HOBs)[33]. Similar studies of Balamurugan et al. showed that the incorporation of 5 mol % of Si into hydroxyapatite enhanced the dissolution rate of the material and increased the proliferation rate of human osteoblast cells compared to undoped HA[34]. The bioactivity of undoped and Si-doped (0.8 wt% and 1.5 wt%) hydroxyapatite was analysed by immersing all the samples in simulated body fluid (SBF). The (0.8 wt%) Si-doped HA showed higher bioactivity and solubility, with increased proliferation of osteoblast cells[35]. Patel et al. reported the in vivo studies of pure HA and 0.8 wt% Si-doped HA in the femoral condyle of rabbits for a period of 23 days. The percentage of new bone growth was higher for Si-doped HA ($37.5 \pm 6\%$) compared to pure HA ($22 \pm 6\%$) confirming the significant role of Si in new bone formation[36]. In another study, pure HA and Si-substituted HA (0.8 and 1.5 wt%) were implanted in an ovine defect model for 6 and 12 weeks. The new bone regeneration was significantly higher for Si-doped HA without any inflammation making it a suitable material for bone graft substitutes[37]. Thus considering the essential role of Mg and Si ions, the bioceramics based on the above material will play an essential role for bone tissue engineering.

3 Synthesis of Magnesium Silicate Bioceramics

Various synthesis routes, such as mechanical activation[38–40], sol–gel[18, 19, 41–43], and hydrothermal[44] methods have been reported (Table 1) for synthesis of magnesium silicate bioceramics for bone regeneration applications. The common difficulty faced during the synthesis of forsterite ceramics was the formation of the intermediate enstatite ($MgSiO_3$) and periclase (MgO) as impurities[45]. To decrease these by-products, researchers have used solid-state method with extended ball milling (9 h). The synthesized powder when compacted and sintered at 1200 °C for 2 h showed phase pure forsterite[10, 17, 46]. In another study, nanocrystalline forsterite powders were prepared via solid-state reaction, using talc ($Mg_3Si_4(OH)_2$) and magnesium oxide (MgO) as the starting precursors. Here, the authors have studied the mechanical properties and microstructure of the prepared ceramics. In the first method, the samples were prepared by mechanical activation method via sonication, and then it was ball milled with varying time and heat treated at different temperatures. In the second method, the same procedures were followed, but the samples were not heat treated before sintering. The authors

Table 1: Review of forsterite synthesis methods, raw materials and sintering temperature.

S. no.	Synthesis methods	Raw materials	Sintering temperature (°C)	Average particle size	References
1	Mechanical activation	Talc ($Mg_3Si_4O_{10}(OH)_2$) and periclase (MgO)	1000 °C and 1200 °C for 1 h	500 nm	51
2	Solid state	$(MgCO_3)_4$, $Mg(OH)_2$. $5H_2O$, SiO_2 and silk fibroin	1350 °C for 4 h	100–300 nm	61
3	Sol–gel	Magnesium nitrate hexahydrate ($Mg(NO_3)_2{\cdot}6H_2O$, silica (SiO_2) and strontium nitrate ($Sr(NO_3)_2$ as dopant	800 °C and 1000 °C for 2 h	20–50 nm	59
4	Sol–gel combustion method	Magnesium nitrate, and tetraethyl orthosilicate	1300 °C for 3 h	–	45
5	Sol–gel	Magnesium nitrate hexahydrated $Mg(NO_3)_2{\cdot}6H_2O$,tetraethyl orthosilicate (TEOS $(C_2H_5O)_4Si$	900 °C for 2 h	10–26 nm	62
6	Mechanical activation	Amorphous SiO_2 and $MgCO_3$	900 °C to 1200 °C for 1 h	< 1000 nm	39
7	Mechanical activation	Talc ($Mg_3Si_4O_{10}(OH)_2$) and magnesium carbonate ($MgCO_3$)	1000 °C to 1200 °C for 1 h	10 µm	38
8	Sol–gel	Magnesium nitrate hexahydrate ($Mg(NO_3)_2{\cdot}6H_2O$, colloidal silica (SiO_2), polyvinyl alcohol, sucrose and nitric acid.	800 °C for 2 h	25–45 nm	41
9	Sol–gel	Hexahydrated magnesium nitrate ($Mg(NO_3)_2{\cdot}6H_2O$, tetraethyl orthosilicate (TEOS-$C_8H_{20}O_4Si$, as raw materials and polyvinyl alcohol (PVA), sucrose and nitric acid as binder and pH regulators	800–1000 °C for 2 h	40 nm	18
10	Precipitation method	Magnesium nitrate hexahydrate, tetraethyl orthosilicate, P123 (EO20PO70EO20) HCl,	600 °C for 3 h	5 nm	65
11	Two-step combustion method	$Mg(NO_3)_2$ magnesium nitrate, (TEOS) tetraethyl orthosilicate, citric acid	800 °C for 1 h	20–50 nm	93
12	Polymer matrix method	Magnesium nitrate ($Mg(NO_3)_2{\cdot}6H_2O$), colloidal silica, PVA, sucrose as a template material	500–1000 °C for 3 h	< 200 nm	50
13	Microwave-assisted	Silica gel and magnesium hydroxide ($Mg(OH)_2$)	500–1200 °C by microwave heating in the air	< 100 nm	54
14	Mechanical activation	Talc and $MgCO_3$ (2:1) ratio	1000 °C for 1 h	30–60 nm	49
15	Solid-state reaction	Magnesium oxide (MgO) and talc ($Mg_3Si_4(OH)_2$)	1200–1500 °C for 2 h	–	47
16	Sol–gel combustion method	Magnesium nitrate, tetraethyl orthosilicate, conc. nitric acid as catalyst, glycine (fuel), urea (fuel)	700–1100 °C for 2 h	< 1 µm	81
17	Mechanical activation	Talc ($Mg_3Si_4H_2O_{12}$) and magnesium carbonate ($MgCO_3$)	1000 °C for 1 h	80–82 nm	94

Table 1: continued

S. no.	Synthesis methods	Raw materials	Sintering temperature (°C)	Average particle size	References
18	Hydrothermal method	Silicon dioxide (SiO_2) and periclase (MgO)	500–1200 °C for 2 h	~234 nm	95
19	Sol–gel and Mechanical activation	Magnesium nitrate and silica, polyvinyl alcohol, sucrose, nitric acid	600 °C-1000 °C for 1 h	30–112 nm	52
20	Microwave irradiation	Magnesium nitrate hexahydrate ($Mg(NO_3)2{\cdot}6H_2O$, tetraethyl orthosilicate (TEOS)	800 °C for 2 h	~100 nm	55
21	Sol–gel/surfactant method	Magnesium methoxide, tetraethyl orthosilicate, toluene/methanol, dodecylamine as a surfactant and tert-butyl amine and water as hydrolysis agents	800 °C for 2 h	25–45 nm	48
22	Sol–gel method	Magnesium nitrate hexahydrate ($Mg(NO_3)_2{\cdot}6H_2O$) and colloidal SiO_2	1110, 1150, 1200 °C for 8 h	5–50 µm	19
23	Sol–gel method	Magnesium nitrate hexahydrate ($Mg(NO_3)_2{\cdot}6H_2O$), tetraethyl orthosilicate (TEOS) and HNO_3	800 °C for 30 min	~27 nm	42
24	Hydrothermal method	Sodium silicate, magnesium nitrate hexahydrate, ethanol and PEG, NaOH	600 °C for 4 h, 8 h and 12 h	–	67
25	Two-step sintering method	$MgCO_3$ and amorphous SiO_2	1300 °C for 6 min and 750 °C for 15 h	20–60 nm	96
26	Sol–gel technique/mechanical activation	Tetraethyl orthosilicate, triethylphosphate and calcium nitrate as sol–gel precursors. 58S bioactive glass ($SiO_2{\cdot}Cao{\cdot}P_2O_5$)	600 °C for 1 h	10–60 nm	60
27	Sol–gel method	Magnesium nitrate hexahydrate, tetraethyl orthosilicate, P123 (EO20PO70EO20) as surfactants	350 °C, 550 °C and 750 °C for 1 h	–	66
28	Mechanical activation technique	Talc ($Mg_3Si_4O_{10}(OH)_2$, magnesium carbonate ($MgCO_3$) and periclase (MgO)	1000 °C and 1200 °C for 1 h	250–350 nm	40
29	Solid-state method	Silicon dioxide, magnesium oxide, strontium oxide and zinc oxide as dopants	1200 °C for 2 h	–	10, 17, 46
30	Sol–gel method	Magnesium salts, colloidal silica, PVA and sucrose	800 °C for 2 h	25–70 nm	71

have showed that formation of secondary phases such as MgO and $MgSiO_3$ can be decreased with increase in ball milling time, sintering temperature and higher amplitude of ultrasonication[47]. Anovitz et al. combined both sol–gel and surfactant method to obtain fine particles of forsterite without any contamination by burning the powder at 800 °C overnight[48].

In a similar study, Tavangarian and Emadi showed that pure forsterite bioceramics can be prepared via the mechanical activation method using ammonium chloride as a catalyst, annealed at 1000 °C for 1 h. The results showed that the synthesized nanostructured forsterite was bioactive and had the ability of apatite formation[49]. Choudhary et al. used sol–gel combustion method to prepare forsterite powder. They used

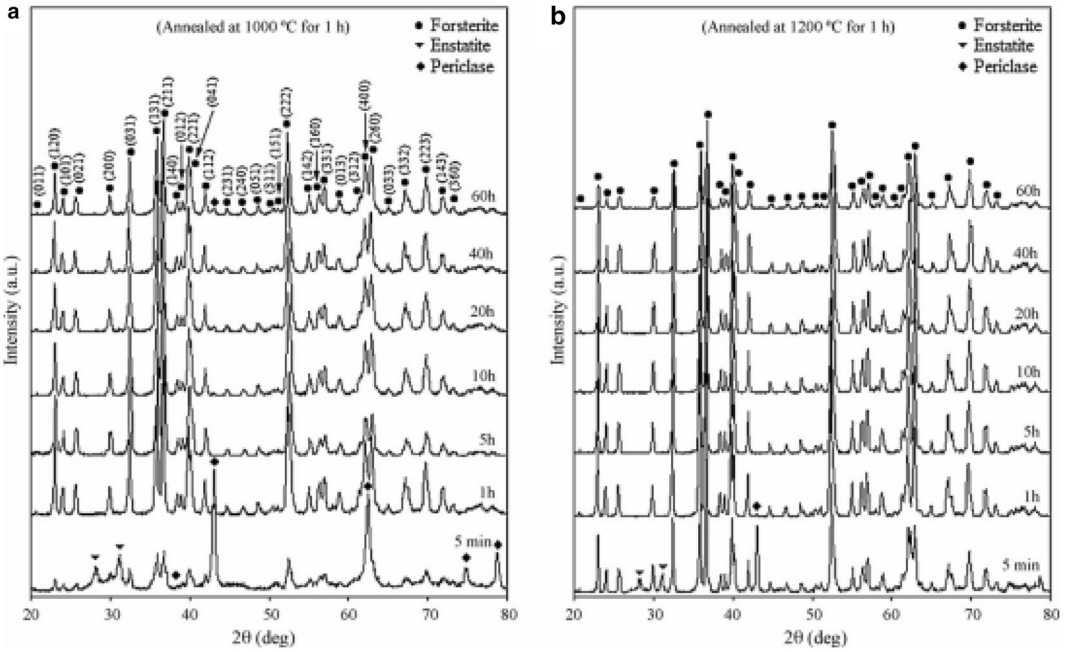

Figure 1: X-ray diffraction patterns of forsterite powders with varying milling time and sintering temperatures annealed **a** at 1000 °C, **b** at 1200 °C for 1 h, from Tavangarian et al.[51]

urea and glycine as two different fuels and studied the degradation properties and antibacterial activity of the synthesized and compacted forsterite bioceramics structures[45]. Saberi et al. synthesized nanocrystalline forsterite powder via cost-effective low temperature polymer matrix method[50]. In a related studies, Tavangarian et al. prepared nanocrystalline forsterite powder by varying the milling time from 5 h up to 60 h and annealed the powder at two different temperatures (1000 °C and 1200 °C) for 1 h[51] [Fig. 1 (reproduced with permission)]. The forsterite phase formation was noticed with increase in milling time up to 5 h and further increase in temperature showed no significant effects on phase formation. The particle size and crystallite size were found to be less than 1 μm and 60 nm, respectively[38, 40, 51].

The combination of sol–gel and mechanical activation method was employed for the synthesis of single-phase nanostructured forsterite powder[52]. The obtained ball milled powder was sintered at low temperature starting from 600 up to 1000 °C for 1 h to get pure nano forsterite powder. With increase in temperature above 750 °C, the formed MgO reacts with the SiO_2 at the surface level and forms enstatite ($MgSiO_3$). Further, the produced MgO diffuses into enstatite particles, resulting in the formation of pure forsterite powder[53]. Research group of Bafrooei et al. synthesized nano forsterite powder through microwave-assisted high-energy ball milling technique. Magnesium hydroxide and silica gel were used as starting materials. The raw powders were milled up to 40 h; further the powders were calcined at 500–1200 °C using microwave heating. The results indicated that at 900 °C, pure single phase forsterite was formed without any other phases such as SiO_2 and MgO. The obtained powders were compacted and sintered using conventional sintering (1150–1350 °C) and microwave sintering (1.1 kW, 2.45 GHz multimode microwave). From the studies, it was concluded that microwave sintered materials showed higher densification with smaller grain size and uniform grain growth[54].

Using a novel cost-effective, low-temperature method, nanocrystalline forsterite was synthesized using magnesium nitrate and sucrose as a template material. The obtained powder was calcined in an electric furnace varying from 500 to 1000 °C for 3 h. Initial crystallization of forsterite was seen at 730 °C and with increase in temperature complete crystallization of the forsterite phase was seen at 800 °C with the average particle size around 200 nm[50]. Recently, Kheradmandfard et al. synthesized pure nano forsterite at low temperature (800 °C) using an ultrafast, green synthesis method via microwave irradiation technique[55]. Magnesium nitrate hexahydrate ($Mg(NO_3)_2{\cdot}6H_2O$) and tetraethyl orthosilicate (TEOS) were used as starting materials. The

reaction mixture was refluxed in a modified microwave oven at 850 W and 2.45 GHz. Further, the mixture was subjected to microwave irradiation for 15 min. The obtained powders were dried at 90 °C for 1 h and sintered at 800 °C for 2 h. The main advantage of this technique is it increased the rate of the reaction and decreased the reaction time period. The average particle size of the prepared forsterite powder was found to be around 100 nm.

3.1 Addition of Dopants

The major advantage of forsterite bioceramics is its controlled degradation behaviour, enhanced mechanical properties and improved biological response. Further, these properties can be tuned by addition of essential cations. Several studies have reported that the incorporation of essential trace elements, such as; manganese (Mn), zinc (Zn), strontium (Sr), silver (Ag) and iron (Fe) in calcium phosphates played an important role in improving the mechanical and biological properties[56–58]. With the scientific understanding of dopant-induced change in biocompatibility of CaPs, a new area of research on doped forsterite had started. Gheitanchi et al. prepared pure forsterite and Sr-doped forsterite nanopowder via the sol–gel route[59]. During the preparation process, the authors used PVA and sucrose to avoid the dissimilarity in hydrolysis and condensation process which bring out inhomogeneity of the reaction. They varied the percentage of Sr from 0, 0.05, 0.1, 0.2 and 0.4 at.% and sintered all the samples at 800 °C and 1000 °C for 2 h. Apart from the forsterite phase, other secondary phases such as $MgSiO_3$, MgO and $Sr_2MgSi_2O_7$ were also observed in the Sr-doped forsterite nanopowder. In a similar research, Devi et al. prepared pure ZnO- (0, 0.25, 0.5 wt%) and SrO (0, 1, 2, 3 wt%)-doped forsterite powder by the solid-state method. The prepared undoped and doped powders were compacted into circular discs and sintered at 1200 °C for 2 h using a muffle furnace. By increasing the dopant composition, the degradation and the porosity of the samples also increased[10, 17, 46].

3.2 Composite Systems

Composite systems particularly in forsterite ceramics are still an underexplored area of research. Forsterite composite systems, particularly with bioglass, silk and polymers, are of particular interest, as the incorporation of these materials increases the potential application fields. Recently, Saqaei et al. fabricated 58S bioactive glass–forsterite nanocomposite using the sol–gel technique. They varied the forsterite powder from 0, 10, 20 and 30 wt% and studied the effect of addition of forsterite nanopowder on the antibacterial and bioactivity behaviour[60]. A novel forsterite/silk fibroin composite was fabricated via the freeze-drying method. Four different kinds of samples were prepared in the ratio of (forsterite/silk fibroin) 0: 100, 20:80, 30:70 and 40:60 and all the prepared samples were freeze dried for 3 days[61]. The new self-curing nano forsterite biocomposites were prepared by combining the forsterite powder (0, 5, 15, 30, 50, 70 wt%) with organic monomer 2,2-bis[4-(2-hydroxy-3-methacryloyloxypropoxy)-phenyl]propane{bis-GMA} and triethyleneglycol dimethacrylate {TEGDMA}. All the fabricated samples showed hydroxyapatite growth with improved mechanical and biological properties[62].

3.3 Influence of Pore Forming Agents

Porosity plays an important role in the overall degradation and biocompatibility of bioceramics. The pore of specific size and distribution helps in implant integration, improves the degradation rate and decreases the implant rejection[63, 64]. The porous nanocomposite material consisting of forsterite nanopowder/polycaprolactone (PCL) was prepared through solvent-casting/particle-leaching method using sodium chloride particles as porogen. The PCL composites with varying (10–50 wt%) forsterite nanopowders were prepared. All the prepared samples were air dried for 48 h to evaporate the solvents completely. The synthesized composites exhibited well-interconnected porous structure with pore size varying from 100 to 400 μm and with the porosities around 90–92%[14]. Mesoporous forsterite with pore size of 5 nm was fabricated using magnesium nitrate hexahydrate and tetraethyl orthosilicate as starting material and P123 (EO20PO70EO20) as template. The prepared disc-shaped samples were calcined at 600 °C for 1 h in air to remove the template. The synthesized mesoporous forsterite showed enhanced degradation, good cytocompatibility, and higher surface area with pore volume of 0.41 cm^3/g[65]. In a similar way, Bigham et al. fabricated ordered mesoporous magnesium silicate (OMMS) via the sol–gel route using P123 (EO20PO70EO20) as a surfactant. The synthesized product was air dried at 50 °C for 24 h and calcined at 350–750 °C for 4 h to remove all the surfactant. The samples calcined at 750 °C showed wider pore size distribution with around 20 nm pore size, making the material suitable

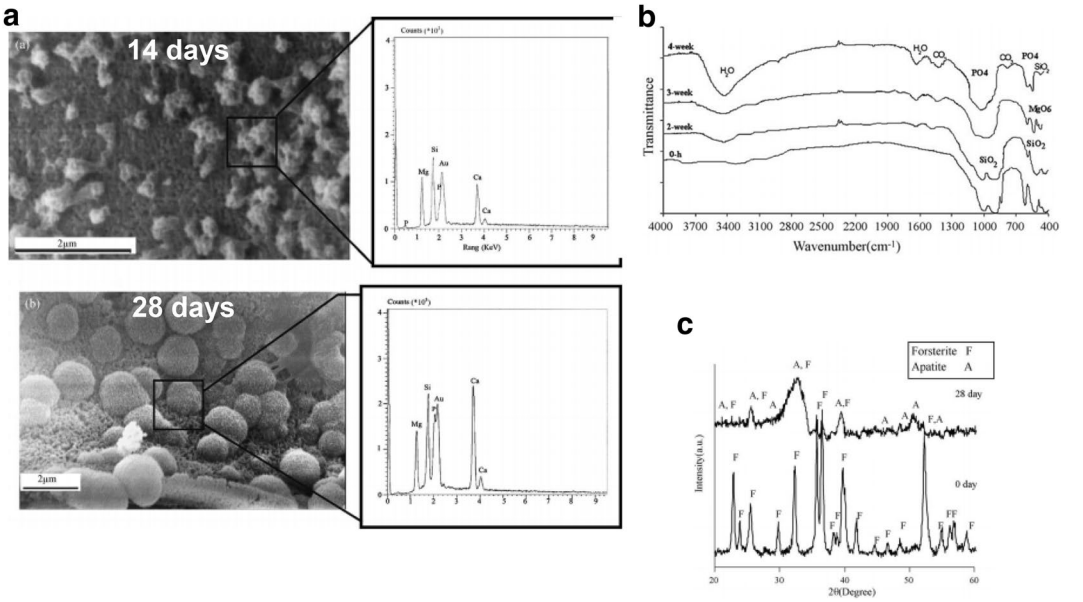

Figure 2: **a** SEM and EDX images. **b** FT-IR spectra. **c** XRD pattern of forsterite nanopowders immersed in SBF for various time points, from Kharaziha et al.[41]

for drug delivery systems[66]. In another study, the authors have prepared mesoporous magnesium silicate via the hydrothermal method using polyethylene glycol (PEG) as surfactant. The resulting mixture was washed several times to remove the inorganic ions and the samples were dried overnight at 90 °C. Finally, all the samples were calcined from 500 to 700 °C for 4 h. On increasing the calcination temperature, the pore size of the samples increased with decrease in surface area[67].

4 In Vitro Behaviour

4.1 Dissolution and Biodegradation Properties

For any clinically adoptable implant, the degradation rate of the material should match the rate of new bone formation. This degradation takes place via two processes: (1) chemical dissolution and (2) cell-mediated resorption. The degradation or dissolution study in the artificial media is a well-known method in which pH, weight loss and ionic release profile are measured with respect to time. Various researchers have suggested that forsterite bioceramic can be employed in bone regeneration applications because of its enhanced degradation rate[22, 62, 65]. Choudhary et al. examined the degradation behaviour of forsterite powders prepared using two different fuels [glycine (FG) and urea (FU)]. They reported that forsterite ceramics when immersed in SBF solution showed weight loss of around 2.8% (FG) and 0.78% (FU) respectively. FG exhibited enhanced weight loss due to smaller particle size and higher surface area compared to FU[45]. Further, Kharaziha and Fathi synthesized forsterite nanopowder with a particle size of 25–45 nm. The authors evaluated the bioactivity of the samples by soaking the forsterite compacts in SBF for up to 28 days and found clusters of agglomerated hydroxyapatite that increased with increase in time [Fig. 2a (reproduced with permission)]. FT-IR spectra showed the characteristic bands of apatite crystals at 1030–1090 cm^{-1}, 574 cm^{-1} and 471 cm^{-1}. The CO_3^{2-}groups of apatite were observed at 1418 cm^{-1}, 1462 cm^{-1} and 872 cm^{-1}. The bands at 3477 cm^{-1} and 1619 cm^{-1} are assigned to be hydroxyl groups in apatite [Fig. 2b (reproduced with permission)]. The XRD pattern confirmed the formation of apatite covering the surface of the forsterite samples [Fig. 2c (reproduced with permission)]. Further, the released concentration of Mg ions in SBF continued to increase, whereas the Ca and P ions gradually decreased confirming the formation of hydroxyapatite layer over the forsterite compacts[41].

In a similar study, Naghiu et al. evaluated the bioactivity of the synthesized nanopowder for 7 and 14 days in SBF solution and found that the forsterite nanoceramics were highly bioactive and biocompatible. After immersion in SBF, the formation of hydroxyapatite was confirmed using FT-IR, SEM–EDX and XRD[18]. The AAS analysis by Tavangarian and Emadi showed that

the nanostructure forsterite bioceramics released Mg ions into the SBF solution, indicating that forsterite bioceramics were biodegradable and bioresorbable, hence making it an excellent material for bone tissue engineering applications[49]. The surface morphology of undoped and forsterite (0, 5, 15, 30, 50, 70 wt%)-doped polymer biocomposites (2,2-bis[4-(2-hydroxy-3-methacryloyloxypropoxy)-phenyl]propane (bis-GMA)/triethyleneglycol dimethacrylate (TEGDMA), before and after immersion in SBF for 0, 14 and 28 days, was analysed using AFM and the images are shown in Fig. 3 (reproduced with permission). From the AFM images, it can be seen that there is an increase in surface roughness for all the samples after 14 days immersion in SBF. The surface roughness (root mean square: RMS) value for undoped and forsterite-doped biocomposites before and after immersion in SBF are shown in Table 2 (reproduced with permission). The pure polymer sample did not show any characteristic morphology even after 28 days of immersion, whereas after 14 days of immersion forsterite/polymer composites showed new fibrous structure because of the presence of forsterite interaction with the SBF solution. After 28 days, there was a significant increase in surface roughness. Some imperfections and slight erosion are seen on the surface of the doped samples because of the deep penetration of SBF[62].

Devi et al. compared the biodegradation property of forsterite with that of commonly used HA and β-TCP ceramics (Table 3). All the sintered samples were immersed in SBF for 8 weeks to evaluate the degradation behaviour. It was found that forsterite bioceramics lost 9 wt% compared to that of 1wt% for β-TCP ceramics, whereas HA samples gained 2.5 wt% after 8 weeks of immersion. These results were further supported by increase in pH and ionic concentration of released Mg ions in the dissolution media[10] [Fig. 4 (reproduced with permission)]. Further, addition of dopants such as Zn and Sr enhanced the degradation property of the ceramics. Upon addition of 0.5 wt% of Zn enhanced the weight loss to 22 wt% when compared to pure forsterite (9%) (Fig. 5). The pH of the dissolution media increased for Zn-doped ceramics because of the higher dissolution rate that was supported by the ionic release profile of Mg ions, which showed threefold release for Zn-doped forsterite ceramics[17]. In a similar way, addition of 3 wt% Sr into forsterite degraded ceramics much faster with a weight loss of 12% compared with pure forsterite (9%) (Fig. 5). The cumulative release profile of Mg^{2+} ions (1300 ppm) and Si^{4+} ions (300 ppm) increased rapidly for 3 wt% Sr after 8 weeks of immersion[10].

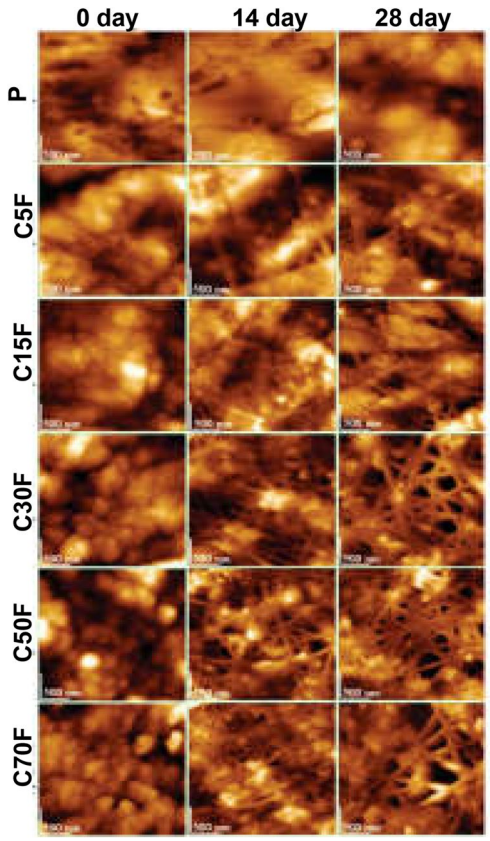

Figure 3: 2D AFM topographies of pure and forsterite/polymer biocomposites before and after immersion in SBF for 14 and 28 days, from Furtos et al.[62]

4.2 Mechanical properties

Mechanical properties of the bioceramics play an important role in determining the stability of the material in vivo for the bone regeneration application. The natural bone has an average compressive strength of around 130–190 MPa of cortical bone and 3.6–9.3 MPa for cancellous bone[68]. When implanted inside the human body, the strength of the designed implant should be similar to that of natural bone. Ni et al. synthesized forsterite powder using the sol–gel method and studied the mechanical properties of the ceramics by varying the sintering temperature and time. At 1350 °C, the bending strength and fracture toughness of forsterite ceramics was found to be 150 ± 8 MPa and 1.8 ± 0.4 Mpa $m^{1/2}$. With increase in the sintering temperature from 1350 to 1450 °C, the bending strength (181 ± 9 MPa) and fracture toughness (2.3 ± 0.1

Table 2: Surface roughness values (RMS) (root mean square) for pure polymer and forsterite/polymer composites before and after immersion in SBF for various days, from Furtos et al.[62]

Sample code	Roughness (RMS) of surface (nm ± SD nm)		
	0 day	14 days	28 days
P	18 ± 2	19 ± 3	39 ± 8
C5F	17 ± 3	47 ± 9	49 ± 9
C15F	21 ± 2	37 ± 5	38 ± 5
C30F	20 ± 3	47 ± 8	51 ± 9
C50F	15 ± 2	42 ± 8	47 ± 6
C70F	18 ± 4	46 ± 3	54 ± 7

Mpa $m^{1/2}$) also increased for these samples. On further increase in temperature from 1450 to 1550 °C, the bending strength (145 ± 8 MPa) and fracture toughness (1.6 ± 0.2 Mpa $m^{1/2}$) of the ceramics decreased due to the formation of flaw structure and grain coarsening which was further confirmed by fractographical analysis. The fracture surface of forsterite ceramics sintered at 1450 °C and 1550 °C is shown in Fig. 6 (reproduced with permission). The samples sintered at 1450 °C showed sharp-edged pores with an average grain size of 10 µm. Further, increasing the temperature up to 1550 °C causes grain growth which traps the pores inside, resulting in decreased mechanical properties. The authors have shown significant improvement in fracture toughness for forsterite samples (2.3 ± 0.0 Mpa $m^{1/2}$) when compared to hydroxyapatite (0.75–1.2 Mpa $m^{1/2}$) ceramics[19].

The forsterite scaffolds prepared using two different fuels, namely glycine (FG) and urea (FU), showed variations in the compressive strength and Young's modulus. Both the samples had superior compressive strength in comparison to natural cortical bone. The FG showed a higher compressive strength (201 MPa) and Young's modulus (4.8 GPa) compared to FU, which has compressive strength of 124 MPa and Young's modulus 4.6 GPa (Fig. 7). This difference in mechanical property was due to difference in particle size. FG had smaller particle with higher surface area compared to FU. These results proved that the compressive strength of the synthesized forsterite scaffolds had better strength compared to cortical bone (130–200 MPa) even after 1 month of soaking time in SBF[45]. Ghomi et al. fabricated porous forsterite scaffolds with interconnected pore size from 50 to 200 µm using the gelcasting method[69]. The compressive strength and the elastic modulus of the prepared forsterite scaffold sintered at 1200 °C for 4 h was found to be 2.43 ± 0.11 MPa and 182 ± 19, respectively, which is close to the compressive strength (2–12 MPa) of cancellous bone[70].

In another research, forsterite powder combined with silk fibroin composite was fabricated using the freeze-drying method. The compressive strength (1.25–4.6 MPa) and modulus (1.3–4.7 MPa) of the composite increased and the porosity of the samples (92–83%) decreased with

Table 3: Summary of degradation behaviour of HA, TCP, undoped and doped forsterite.

Material composition	Degradation media	Duration (days)	% wt. loss/gain	References
HA	SBF	56	2.59 gain	10
TCP	SBF	56	0.15	10
MgS	SBF	56	8.98	10
MgS/SF (0/100)	PBS	28	18	61
MgS/SF (20/80)	PBS	28	24	61
MgS/SF (30/70)	PBS	28	25	61
MgS/SF (40/60)	PBS	28	30	61
MgS-1Sr	SBF	56	12.8	10
MgS-2Sr	SBF	56	11.8	10
MgS-3Sr	SBF	56	12.5	10
MgS-0.25Zn	SBF	56	14.5	17
MgS-0.5Zn	SBF	56	23.8	17
MgS (FG)	SBF	30	2.8	45
MgS (FU)	SBF	30	0.78	45

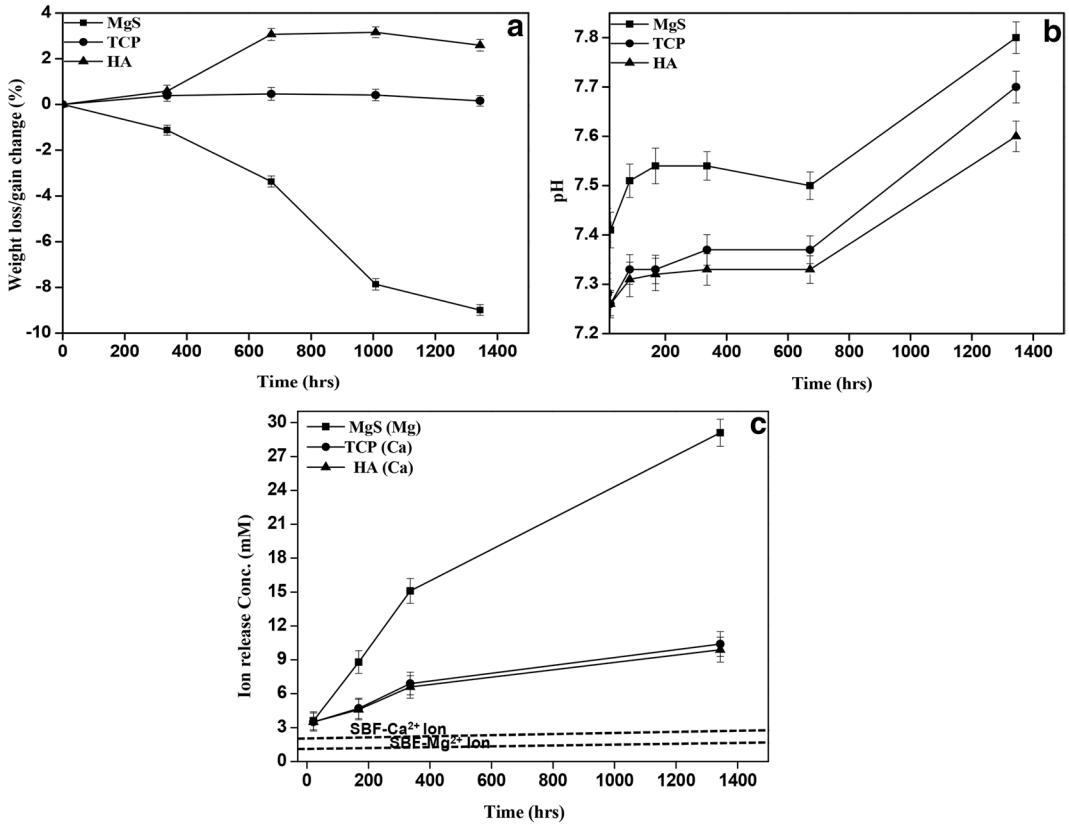

Figure 4: Comparison of the degradation behaviour of forsterite, HA and β-TCP **a** weight loss, **b** change in pH and **c** dissolution of released (Mg^{2+}) (Ca^{2+}) ion concentration at various time points, from Devi et al.[10]

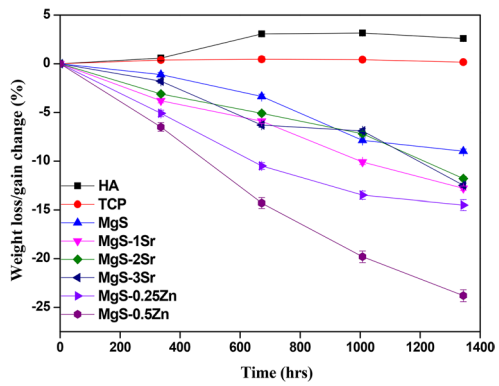

Figure 5: Weight loss/gain behaviour of released HA, TCP, doped Zn and Sr ions at different time points, from Devi et al.[10, 17]

addition of forsterite powder from 0 to 40 wt% [Fig. 8a–c (reproduced with permission)]. The authors found that the decrease in pore size and increase in the particle wall thickness were the major reasons for improvement in the mechanical properties of the composite scaffolds compared to pure silk fibron[61]. The dense two-step sintered (TSS) nanostructured forsterite powder with the crystallite size of 30–45 nm was prepared via the sol–gel method. The sintering behaviour and the mechanical properties (hardness and fracture toughness) are well studied. The results showed that with increase in soaking temperature from 750 to 850 °C for 5 h, both the fracture toughness (1.10 ± 0.5 MPa $^{m1/2}$ to 4.3 ± 0.19 MPa $^{m1/2}$) and hardness (520 ± 45 Hv to 1102 ± 25 Hv) values increased. This increase in fracture toughness could be due to dense forsterite powder and sintering temperature of the powder via the two-step sintering method[71]. These results were best in comparison with Ni et al., who prepared forsterite samples from coarse grain powder and obtained lower fracture toughness of 2.4 MPa $^{m1/2}$. Overall, it was found that the fracture toughness of the dense forsterite ceramics ($K_{IC} = 4.3$ MPa $m^{1/2}$) is better than that of hydroxyapatite ceramics ($K_{IC} = 0.75$–1.2 MPa $m^{1/2}$)[19].

The nanoporous scaffolds comprising nano forsterite with polycaprolactone (PCL) were synthesized by the solvent-casting/particle-leaching method. The effects of the addition

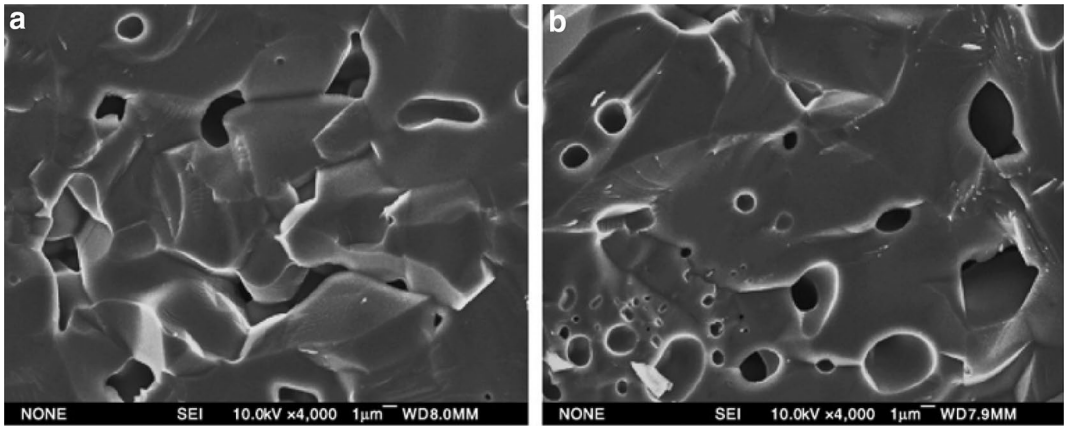

Figure 6: SEM micrographs of fracture surface of forsterite ceramics after sintering at two different temperatures at **a** 1450 °C and **b** 1550 °C for 8 h, from Ni et al.[19]

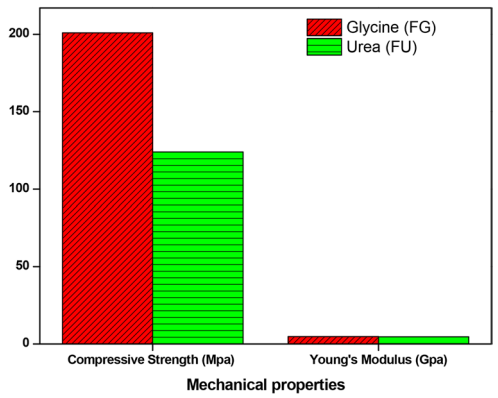

Figure 7: Compressive strength and Young's modulus of forsterite prepared using glycine and urea as different fuels, from Choudhary et al.[45]

of nano forsterite powder varying from 0, 10, 20, 30, 40 and 50 wt% in the PCL were investigated. SEM micrographs of pure PCL and PCL–forsterite composite are shown in Fig. 9 (reproduced with permission). Pure PCL showed macroporous structure with the pores varying from 100 to 400 μm with 92.65% of porosity. With increase in forsterite powder (0–30 wt%), the porosity decreased to 91.38% with the open pores of about 100–300 μm. In addition to macropores, the composite scaffolds possess plenty of micropores (1–10 μm) with rough uneven surface walls. This open and porous interconnected structure enables the transportation and proliferation of osteoblasts cells, making it a suitable candidate for bone tissue engineering applications[14]. In a related studies, Furtos et al. investigated the novel forsterite biocomposite by mixing forsterite powder (5, 15, 30, 50 and 70 wt%) with 2,2-bis[4-(2-hydroxy-3-methacryloyloxypropoxy)-phenyl]propane (bis-GMA) and triethyleneglycol dimethacrylate (TEGDMA) monomers. Upon addition of forsterite powder from 0 to 50 wt%, the compressive strength (128.70 ± 12.90–167.49 ± 10.15 MPa), flexural strength (80.55 ± 12.51–83.20 ± 6.55 MPa) and diametral tensile strength (29.72 ± 2.70–31.55 ± 2.75 MPa) increased, whereas the compressive modulus (1.49 ± 0.20–2.75 ± 0.23 MPa) and flexural modulus (1.94 ± 0.60–7.37 ± 1.85 MPa) increased up to 70% addition of forsterite. Above 50 wt% addition, the compressive strength (147.49 ± 20.84 MPa), flexural strength (59.47 ± 9.81 MPa) and diametral tensile strength (25.45 ± 2.54 MPa) decreased as the excessive powder became a rigid filler, causing phase segregation and bringing more stress inside the polymer matrix[62]. These results are also in line with other published results[72,73].

In a recent research, Devi et al. prepared pure forsterite, Zn- and Sr-doped forsterite using the solid-state method. The porosity, pore and materials distribution of all the samples before and after immersion in SBF for 8 weeks were analysed using 3D-micro-CT and are represented in Fig. 10 (reproduced with permission). Addition of dopants (Sr and Zn) increased the porosity from 1.15% (pure forsterite) to 1.80% (0.25 wt% Zn), 2.29% (0.5 wt% Zn), 1.70% (1 wt% Sr), 1.79% (2 wt% Sr) and 3.06% (3 wt% Sr), respectively. Similarly, because of enhanced dissolution and degradation behaviour of the forstertie samples, the porosity increased after 8 weeks of immersion for all the samples [(2.03% pure forsterite) (2.63% 0.25 wt% Zn) (2.53% − 0.5 wt% Zn) (2.63% − 1

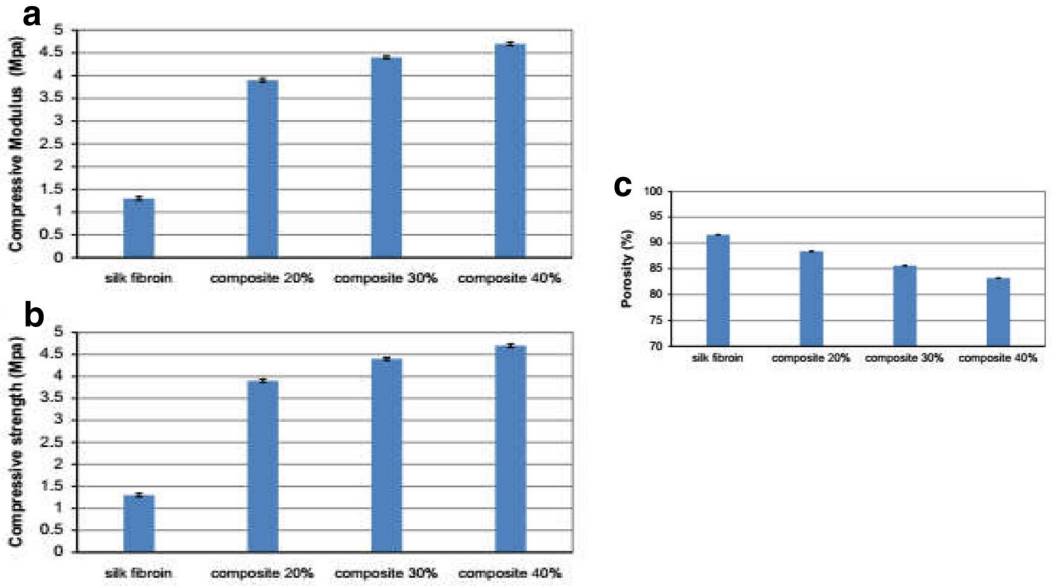

Figure 8: Mechanical properties of silk fibroin and silk fibroin/forsterite composite scaffolds. **a** Compressive modulus, **b** compressive strength and **c** porosity values, from Teimouri et al.[61]

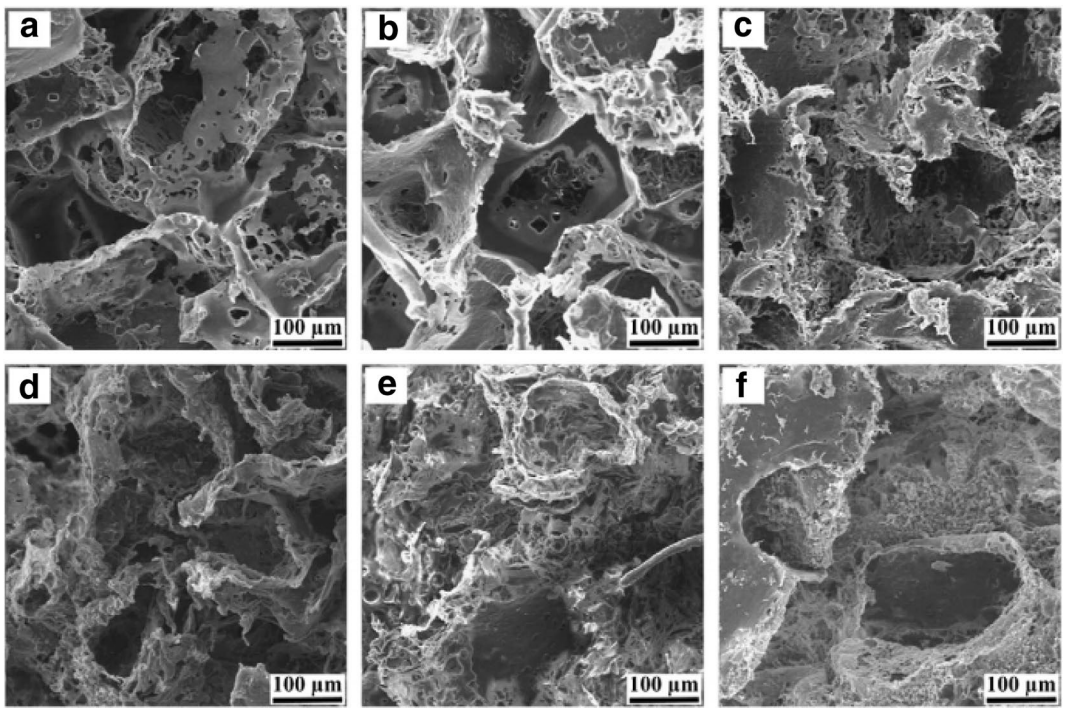

Figure 9: SEM micrographs of surface morphology of **a** pure PCL, **b** PCL-10 wt% forsterite, **c** PCL-20 wt% forsterite, **d** PCL-30 wt% forsterite, **e** PCL-40 wt% forsterite and **f** PCL-50 wt% forsterite, from Diba et al.[14]

wt% Sr), (3.00% − 2 wt% Sr) and (4.53% 3 wt% Sr)]. The interconnected pore size was found to be in the range of 510–580 µm for 0 week samples and 730–790 µm for subsequent 8 weeks immersion in SBF[10, 17, 46].

4.3 Cytocompatibility

In vitro cytocompatibility of magnesium silicate bioceramics, for bone tissue engineering applications, has been widely studied. The most

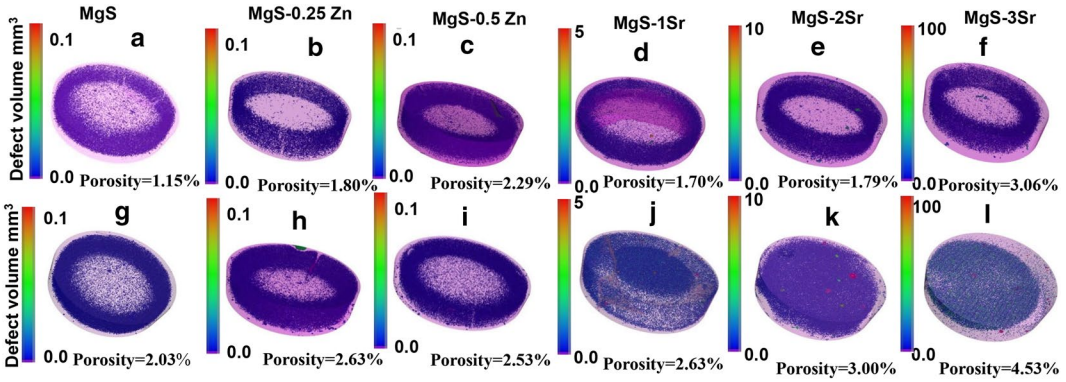

Figure 10: 3D Micro-CT images of the porosity, pore and materials distribution of pure, Zn- and Sr-doped forsterite before (**a**–**f**) and after immersion (**g**–**l**) in SBF, from Devi et al.[10, 17]

commonly used cells were G292, MG-63 and MC3T3-E1 cells. Gheitanchi et al. evaluated the bioactivity of nano forsterite ceramics using MG63 osteoblast cells. The MTT assay showed that both pure forsterite and Sr forsterite samples gradually increased the MG63 proliferation from day 1 to day 7[59]. Similar study of Furtos et al. showed that the incorporation of nano forsterite powder (0, 5, 15, 30, 50 wt%) in the bis-GMA/TEGDMA polymer matrix increased the Saos-2 viable cells from 57.8%±24.4% (0% forsterite only polymer, P) to 82.6%±6.6% for 50% forsterite powder after day 1. After 14 days, all the samples were examined using fluorescence microscopy (Fig. 11 (reproduced with permission) after live/dead staining which showed the complete coverage of viable and well attached cells for all the forsterite biocomposites compared to the undoped polymer matrix[62]. The MTT assay on forsterite powder with varying concentrations (6.25%, 12.5 and 25%) and days (1, 2 and 5 days) showed that the proliferation rate of U20s-type osteoblasts cells increased confirming the absence of cytotoxicity on all the samples[18]. Krishnamurithy et al. synthesized nanocrystalline forsterite powder via the sol–gel combustion route using urea as fuel (FU)[74]. The authors evaluated the in vitro biocompatibility and osteogenic differentiation properties. The forsterite samples seeded with human bone marrow-derived mesenchymal stromal cells (hBMSCs) were compared with commercial bone substitutes (cBS). The hBMSCs had completely colonized the surface of the forsterite scaffold compared to cBS confirming that the degraded products of forsterite were biocompatible and showed the positive way for cell attachment and proliferation. The F-actin analysis depicted that hBMSCs seeded on forsterite samples have underwent actin cytoskeleton remodelling to interact with the forsterite samples. From this phenomenon, we can confirm that the surface chemistry of forsterite was favourable for cell attachment[75]. Further, the authors analysed the osteogenic intra- and extracellular protein expression. Increased BMP2 protein secretion was noticed for hBMSCs seeded onto forsterite (day 1 and 14) when compared to cBS. This analysis showed that the hBMSCs seeded onto forsterite were committed to the pre-osteoblastic lineage. A significant expression of Col1 (both day 1 and 14) in hBMSCs seeded onto forsterite was observed compared to cBS. The substantial enhancement of cells secreting Osterix (OSX) was seen from day 1 to day 14 for forsterite scaffold compared to cBS. Further, the OPN matrix secretion was two times and eight times higher on day 14 and day 1 when hBMSCs were seeded on forsterite scaffold and cBS, respectively. These results supported that forsterite scaffold had greater potential to induce hBMSCs differentiation into osteogenic lineage compared to cBS. Similar research findings were seen when BMP2 expression on hBMSCs was higher when seeded on magnesium phosphate ceramics[76]. The released magnesium ions helped in promoting hMSCs differentiation via the Wnt signalling pathway[77].

In a similar way, the proliferation of MC3T3-E1 cells on TCP, forsterite and mesoporous forsterite samples was evaluated using the MTT assay. The optical density (OD) [Fig. 12a(a) (reproduced with permission)] values of both mesoporous forsterite and forsterite were found to be increased after 7 days of culture compared to TCP showing good cytocompatibility of the samples. In the same study, ALP activity of MC3T3-E1 cells (Fig. 12a(b) on mesoporous forsterite sample after 7 days showed significantly

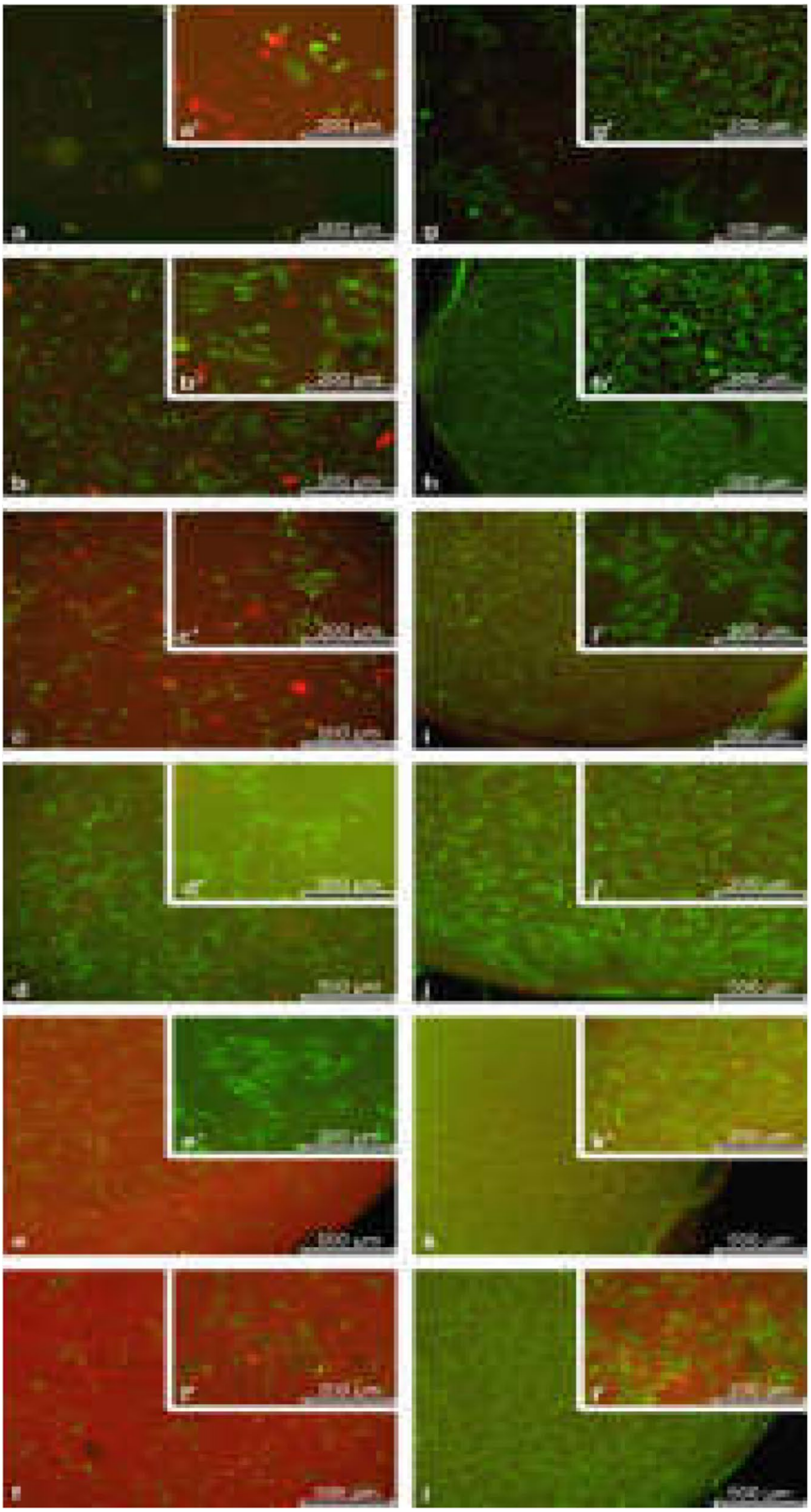

Figure 11: Fluorescence microscopy of Saos-2 cells cultured on discs for day 1 (**a**–**f**, **a´**–**f´**), day 7 (**g´**–**l´**) and day 14 (**g**–**l**). P (**a**, **a´**, **g**, **g´**), C5F-(**b**, **b´**, **h**, **h´**), C15F-(**c**, **c´**, **i**, **i´**), C30F-(**d**, **d´**, **j**, **j´**), C50F-(**e**, **e´**, **k**, **k´**), C70F-(**f**, **f´**, **l**, **l´**), from Furtos et al.[62]

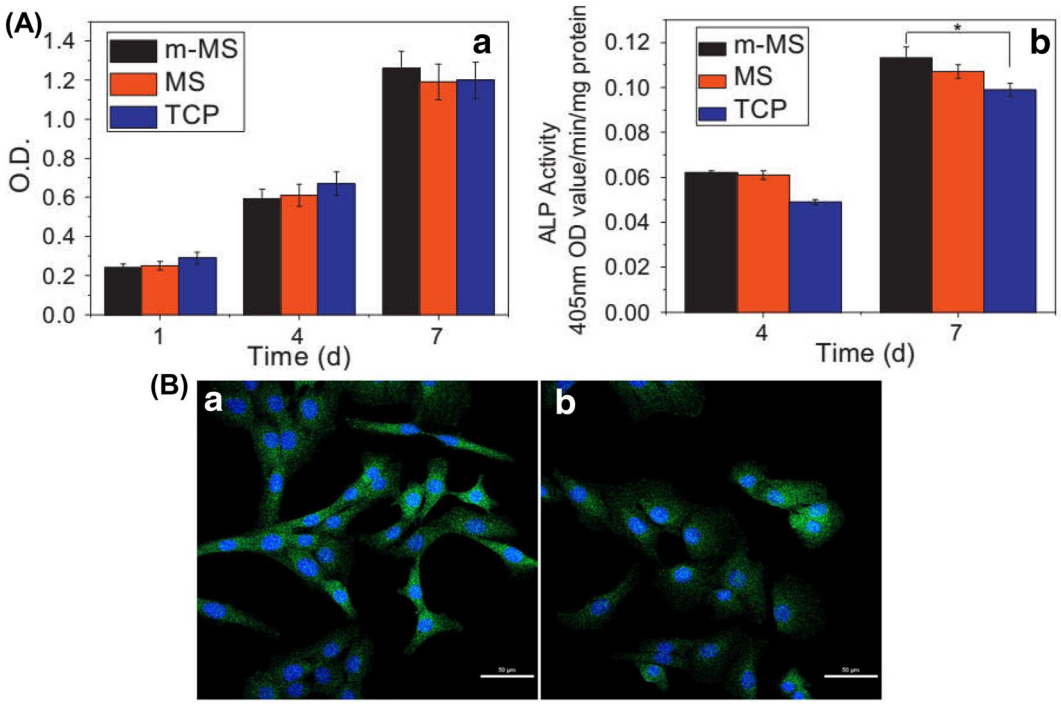

Figure 12: **a (a)** OD values of MC3T3-E1 cells on mesoporous forsterite, forsterite and TCP at 1,4 and 7 days **(b)** ALP activity of MC3T3-E1 cells on mesoporous forsterite, forsterite and TCP at 4 and 7 days. **b** Images of cytoskeletal morphology and spreading of MC3T3-E1 cells, **(a)** mesoporous forsterite and **(b)** forsterite after 4 days using confocal scanning microscopy (scale bar 50 μm), from Wu et al.[65]

higher expression compared to TCP. The cell morphology of MC3T3-E1 cells [Fig. 12b (reproduced with permission)] on mesoporous forsterite exhibited well-flattened structure indicating no negative effect on cell viability or morphology. Thus, mesoporous forsterites are excellent candidates for bone tissue engineering applications[65].

Bigham et al. fabricated ordered mesoporous magnesium silicate (OMMS) using the sol–gel route and investigated the effect of calcination temperature on drug delivery property. The cell viability of all the samples with different calcination temperatures (350 °C, 550 °C, 750 °C) was investigated by osteosarcoma cell line (MG63) using MTT assay and it was found that all the samples showed no toxicity. The results indicated possible usage of the OMMS as drug carriers[66]. The biocompatibility of the forsterite ceramics was evaluated by Ni et al. who showed that at 7 days, a higher proliferation rate of G292 osteoblast cells was noticed[19]. An ultrafast, green synthesis method of nano forsterite showed no toxicity with improved cell proliferation. The ALP activity (Fig. 13a) (reproduced with permission) at day 7 and 14 improved the proliferation and differentiation of MG63 osteoblast cells compared to the control. SEM micrographs of cell morphology (Fig. 13b) (reproduced with permission) showed well-attached polygonal flattened and completely covered MG63 osteoblast cells on the forsterite samples. The dissoluted Mg and Si ions from forsterite powder induced the osteogenic differentiation of MG63 cells through up-regulating the expression of collagen and extracellular matrix proteins[78–80]. The antibacterial activity of forsterite synthesized using two different fuels [glycine (FG) and urea (FU)] was analysed (Fig. 14) (reproduced with permission) against biofilm forming bacteria, such as *S. aureus* and *E.coli.* The authors reported that *S. aureus* was inhibited more than *E.coli* and the bacterial activity was higher for FG because of the enhanced surface properties such as surface area and particle size. The surface area and particle size of FG were found to be higher (65.1 m^2/g) (28 nm) than that of FU (0.93 m^2/g) (1.9 μm), respectively. Thus these results confirmed that forsterite can be used to prevent bacterial infection during surgeries and inhibit biofilm formation in medical implants[81].

In our recent research, the cytocompatibility of pure Zn (0.25 wt% and 0.5 wt%) and Sr (1

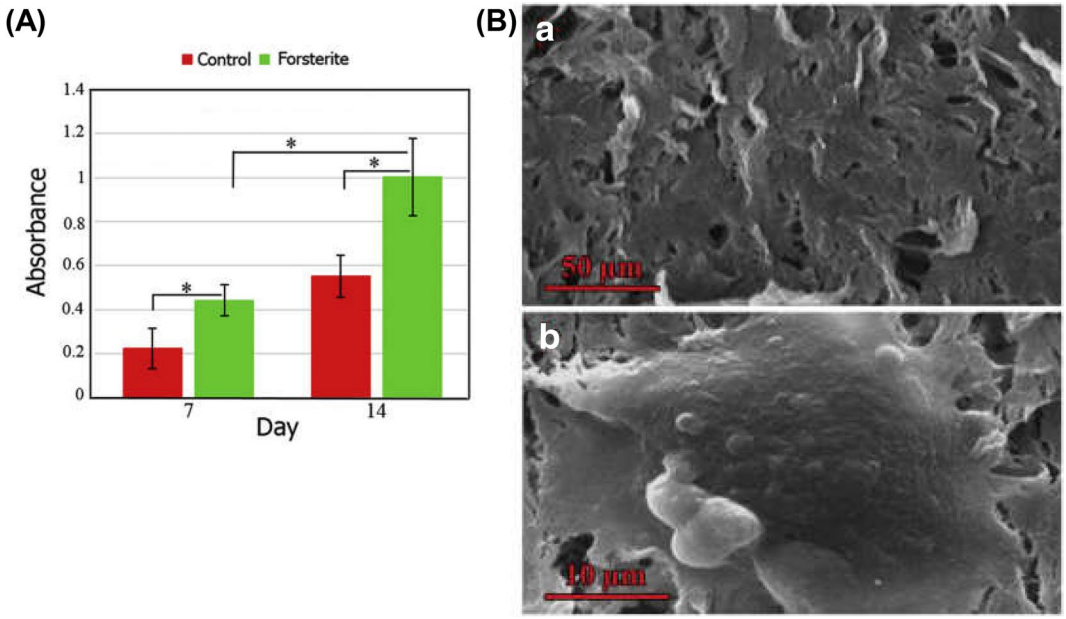

Figure 13: **a** ALP activity of MG63 cells cultured on forsterite and control after 7 and 14 days [*significant difference among the groups ($p < 0.05$)]. **b** SEM micrographs of MG63 cells cultured on forsterite sample after 2 days of culture, from Kheradmandfard et al.[55]

wt%, 2 wt%, 3 wt%)-doped forsterite was analysed using MC3T3-E1 cells at day 1 and day 3 and the results are shown in Fig. 15a (reproduced with permission). The fluorescence images of MC3T3-E1 after day 1 and day 3 presented similar cell attachment for pure and Zn-doped forsterite when compared with the control plate. The DNA quantification after day 3 showed significant increase in cell proliferation for forsterite and Zn-doped forsterite samples[17] [Fig. 15b (reproduced with permission)]. In a similar way, we carried out the MC3T3-E1 cell proliferation of undoped and Sr-doped forsterite samples via DNA quantification [Fig. 15c (reproduced with permission)]. The cell proliferation rate of pure and Sr-doped forsterite samples was found to be increased with increase in culture time, in accordance with live/dead images which showed enhanced live cells on all the samples compared to the control[10] These results confirmed that enhanced degradation behaviour of forsterite with and without any dopant showed good cell attachment and proliferation, rate making it a material suitable for biodegradable bone replacement.

5 In Vivo Biocompatibility

Although one of the most important characterizations, in vivo biocompatibility of magnesium silicate bioceramics has rarely been evaluated. Very few literature exists on in vivo degradability and bone regeneration capability of these new class of bioceramics. In their recent work, Devi et al. for the first time investigated in vivo osteogenesis of pure forsterite, Zn (0.25 wt% and 0.5 wt%)[46] and Sr (1 wt%, 2 wt% and 3 wt%)[10] -doped forsterite samples by implanting the ceramics for 30, 60 and 90 days in the distal femur of white New Zealand rabbits. After the particular interval of time, the postoperated bone samples were studied for bone–implant interface. X-ray radiographs showed the loss in radio-opacity of all the ceramics indicating the enhanced degradation of the ceramics in vivo. After 90 days of implantation, the gradual bone regeneration was noticed in pure, Zn- and Sr-doped forsterite samples. Further, SEM [Fig. 16a (reproduced with permission)] was utilized to understand the bone–implant interfacial bridging. The 90 days images of Zn-doped forsterite implants showed thicker bone formation surrounding the implant material. The 90 days Sr-doped forsterite series indicated a strong fissure gap between the implant and bone. The thick interfacial new bone growth confirmed the binding properties of forsterite ceramics. The 3D micro-CT was used to study the detailed bone growth on the implanted ceramics. After 30 days, degradation on all the samples was noticed and bone started to regenerate on all the ceramics, confirming the osteoconductive property of the ceramics. Within 90 days, the new bone formed had undergone

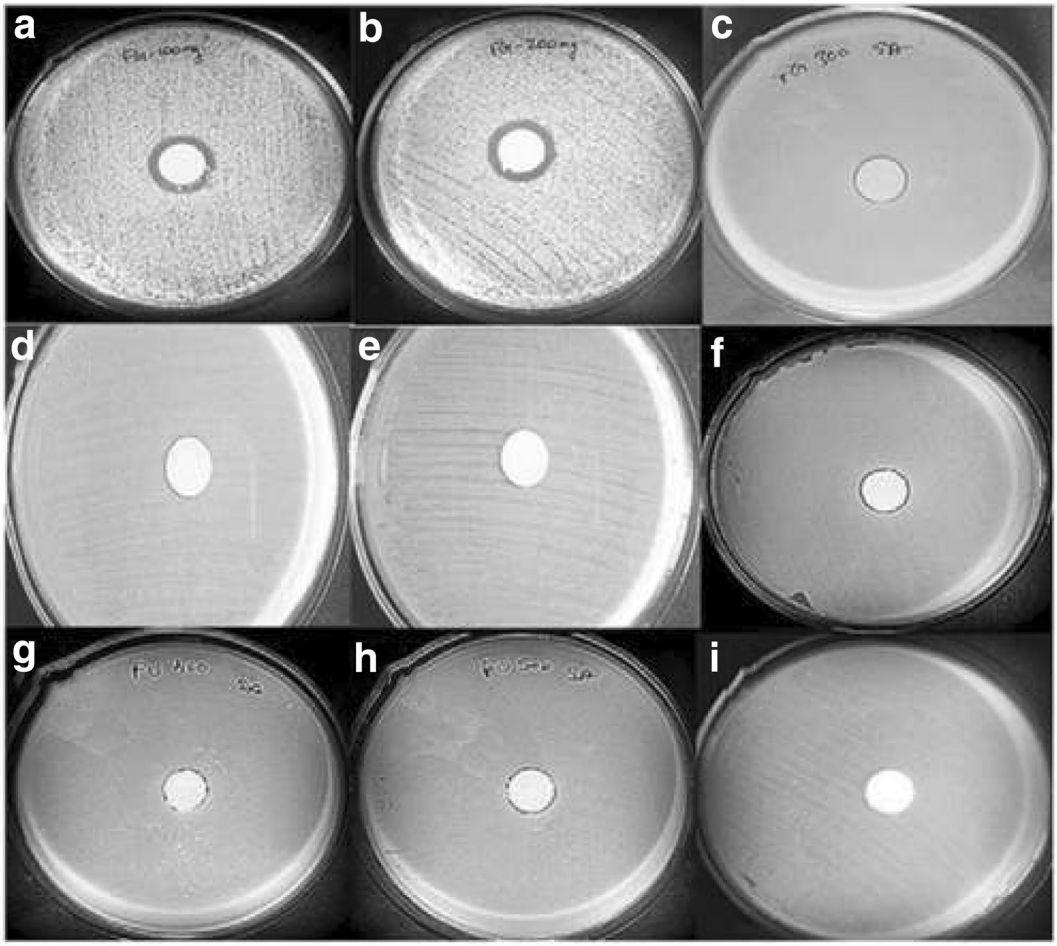

Figure 14: Antibacterial activities of forsterite ceramics prepared using two different fuels glycine (FG) and urea (FU) against *S. aureus* and *E. coli*. FG with *S. aureus* **a** 100 mg, **b** 200 mg, **c** 300 mg, FG with *E. coli* **d** 200 mg, **e** 300 mg and FU against *S. aureus* **f** 300 mg, **g** 400 mg, **h** 500 mg, and FU with *E. coli* **i** 300 mg, from Choudhary et al.[81]

remodelling, which was revealed from the structural arrangement of bone [Fig. 16b (reproduced with permission)]. At 90 days, most of the ceramic material was found to be replaced by new trabecular bone. The enhanced dissolution behaviour of forsterite released Mg and Si ion in the vicinity of the implants. These released ions played a very important role in improving the bone formation in vivo[26, 31, 82, 83].

The percentage of new bone formation was analysed using oxytetracycline (OTC) labelling and is shown in Figs. 17a, 18 and Table 4 (reproduced with permission). At 30 days, golden yellow fluorescence was seen in all the samples. At 90 days, an abundance of new patches of golden yellow fluorescence was noticed over all the samples and the percentage of new bone growth was calculated to be $42 \pm 3\%$ (pure forsterite), $51 \pm 2\%$ (Zn-0.25), $72 \pm 3\%$ (Zn-0.5), $48 \pm 3\%$ (Sr-1), $80 \pm 2\%$ (Sr-2), $75 \pm 2\%$ (Sr-3) for pure and doped forsterite samples, respectively. The detailed H&E stained histological micrographs [Fig. 17b (reproduced with permission)] of undoped, Zn- and Sr-doped forsterite showed enormous amount of new bone regeneration with proliferating osteoblast cells. To study the toxicity of the samples, we carried out the histological studies [Fig. 19 (reproduced with permission)] of three major organs, namely, the heart, kidney and liver. The H&E staining of heart depicted normal musculature confirming that forsterite ceramics have no harmful side effects. The kidney and liver structure do not show any major abnormal changes, indicating no toxic effects on all the samples. Thus, our research group, for the first time, evaluated the complete in vivo biocompatibility of forsterite bioceramics and their ability in promoting new bone formation.

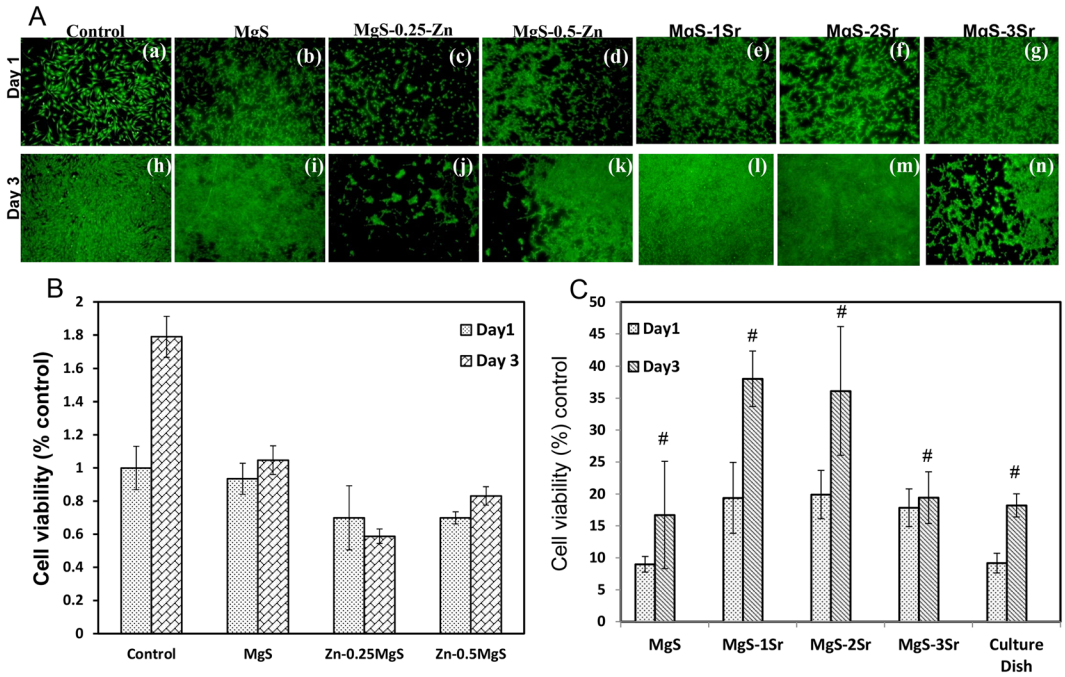

Figure 15: **a** Live/dead images of MC3T3-E1 cells of undoped, Zn- and Sr-doped forsterite after day 1 (**a**–**g**) and day 3 (**h**–**n**) (scale bar = 300 μm). **b**, **c** DNA assay normalized to day 1 of control (#statistical significance), from Devi et al.[10, 17.]

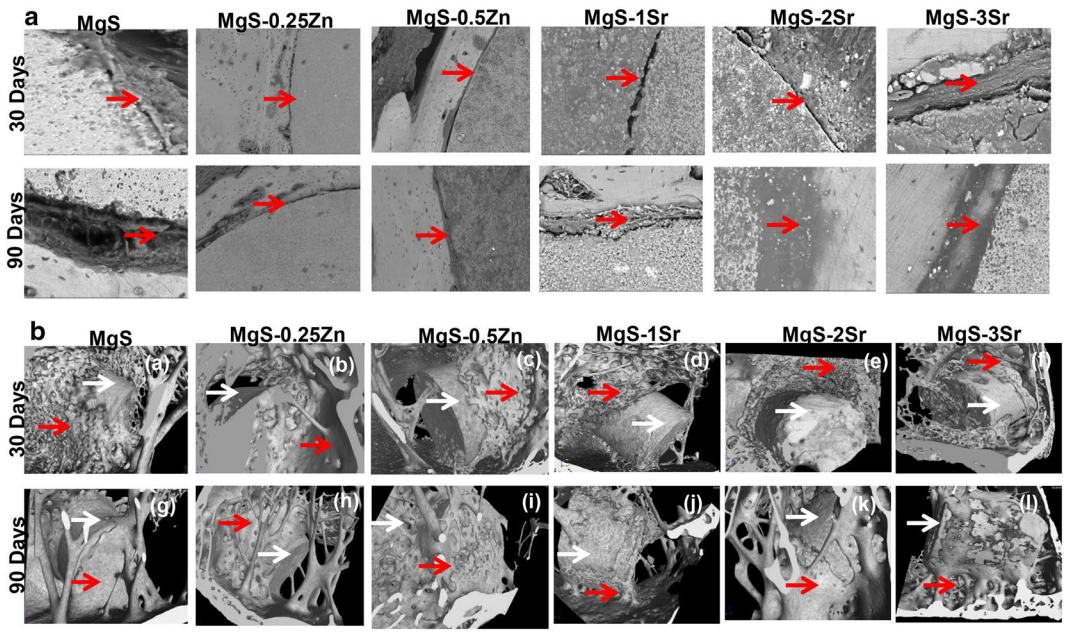

Figure 16: **a** SEM images of bone implant interface of pure, Zn- and Sr-doped forsterite (scale bar = 30 μm) (red arrow showing the interface of bone and implant). **b** 3D micrographs showing new bone regeneration around the implant material for undoped, Zn- and Sr-doped forsterite for 30 (**a**–**f**) and 90 (**g**–**l**) days (red arrow showing the new bone formation and white arrow showing the implant material), from Devi et al.[10, 46.]

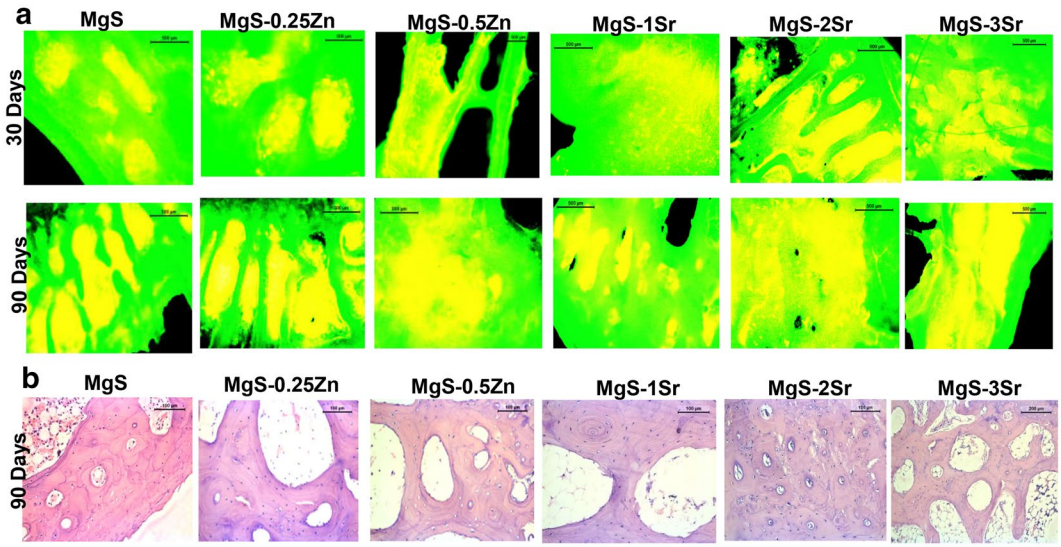

Figure 17: **a** Fluorescence images of bone–implant interface of pure, Zn- and Sr-doped forsterite after 30 and 90 days (scale bar = 500 μm). **b** Histological H&E stained micrographs of pure, Zn and Sr forsterite implanted bone at 90 days (scale bar = 100 μm), from Devi et al.[10, 46].

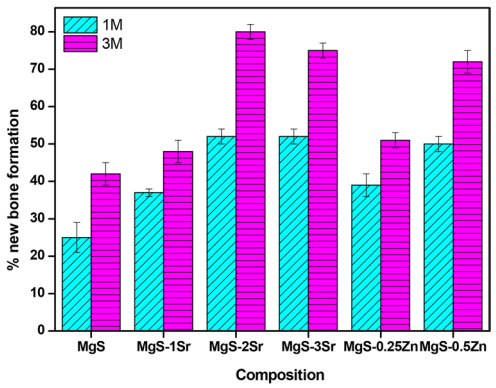

Figure 18: Percentage of new bone formation in the defect site of Zn- and Sr-doped MgS with varying composition and time period, from Devi et al.[10, 46].

6 Other Magnesium-Based Silicate Ceramics for Biomedical Applications

The widespread application of magnesium-containing silicate ceramics is an emerging area of research in the biomedical field. Apart from forsterite, other magnesium-containing silicate ceramics such as akermanite ($Ca_2MgSi_2O_7$), bredigite ($Ca_7Mg(SiO_4)_4$), diopside ($CaMgSi_2O_6$), merwinite ($Ca_3Mg(SiO_4)_2$), monticellite ($CaMgSiO_4$) and proto-enstatite ($MgSiO_3$) have also been reported as potential bioceramics for bone tissue engineering applications[84]. In particular, akermanite, diopside and merwinite have recently drawn special attention because of their superior in vitro and in vivo biological properties[22, 85, 86]. The mechanical properties of merwinite and monticellite are similar to that of cortical bone[85, 87]. The dissoluted products of these materials further increased the osteoblast cell adhesion, proliferation and differentiation[85]. The incorporation of 2–10 wt% of merwinite nanoparticles in β-tricalcium phosphate (β-TCP) increased the mechanical strength and bioactivity compared to undoped β-TCP[88]. The in vivo studies in rat femoral defect model proved that the merwinite promoted osteogenesis and the rate of new bone regeneration was much faster compared to control (β-TCP), thereby making the material suitable for bone replacement[89]. Further, Jin et al. investigated the biocompatibility of enstatite up to 14 days in SBF and showed that enstatite could not induce hydroxyapatite growth. It is reported that the Mg ions are effective inhibitors of apatite nucleation and growth[90, 91]; however, the degraded products promoted the proliferation of mouse fibroblasts (L929 cell) than on traditional hydroxyapatite ceramics[92].

7 Conclusions and Future Directions

The present review summarizes the synthesis methods and mechanical, in vitro and in vivo properties of magnesium silicate degradable bioceramics. With the considerable number of research findings, use of magnesium-based silicate bioceramics

Table 4 Summary of mechanical and biological properties of forsterite

S. no	Preparatory methods	Mechanical properties	Biological properties	References
1	Nano forsterite powders were prepared using sol–gel method	–	Surface morphology of nano forsterite powder showed HA growth after 7 and 28 days in SBF MTT assay showed increase in proliferation of U20S-osteoblast cells without any toxic effect	18
2	Nanostructure forsterite powder was prepared by solid-state method	–	Surface morphology of forsterite samples after immersion in SBF for 14 and 28 days showed cauliflower shape HA. EDX spectra confirmed the presence of Ca and P	49
3	Nano crystalline forsterite powders were synthesized by mechanical activation method	The fracture toughness and microhardness are found to be 3.61 ± 0.1 MPa $m^{1/2}$ and 940 ± 10 Hv respectively	–	96
4	Undoped and Zn-doped (0.25 and 0.5 wt%) forsterite bioceramics were prepared by solid-state method	–	The surface morphology of pure and Zn-doped forsterite ceramics showed uniform degradation for all the samples after 8 weeks of immersion in SBF solution. The 3D-micro-CT showed porosity of around 1.15% for forsterite and 2.3% for Zn-doped forsterite The 2D micro-CT showed uniform pore distribution with the pore size of 30–140 µm irrespective of sample composition MC3T3 cells showed good proliferation on all the samples compared to control. Further, DNA quantification at day 1 and 3 showed increased proliferation on all the samples The in vivo bone regeneration in rabbit model showed improved bone formation for all the samples as confirmed from SEM, micro-CT and quantitatively by oxytetracycline labelling. The percentage of new bone formation after 90 days for Pure forsterite, 0.25 Zn- and 0.5 Zn-doped forsterite was found to be $42 \pm 3\%$, $51 \pm 2\%$ and $72 \pm 2\%$ respectively. Further, the histological analysis of vital organs like heart, kidney and liver showed normal tissue responses after 90 days of implantation in rabbit model	17, 46
5	Pure forsterite and forsterite/silk fibroin composites were prepared through freeze-drying method	Addition of 40 wt% forsterite powder in silk fibroin increased the Compressive modulus from 1.2 to 4.7 MPa and compressive strength from 1.3 to 4.6 MPa	Macropores in the range of 30–120 µm	61
6	Undoped and Sr-doped (0, 0.05, 0.1, 0.2 and 0.4 at %) forsterite nanopowders were synthesized by sol–gel route	–	Cauliflower like structure we seen on the surface of pure and Sr-doped forsterite after soaking in SBF for 28 days. EDX confirmed the presence of Ca and P The MTT assay showed increase in proliferation of MG63 cells for all the samples from day 1 to day 7	59

Table 4 continued

S. no	Preparatory methods	Mechanical properties	Biological properties	References
7	Pure and bioactive glass (58S)-forsterite nanocomposite powders (10, 20 and 30 wt%) were prepared by sol–gel method	–	The 20 wt% of forsterite into bioglass showed the maximum number of apatite clusters on the surface of the sample after 28 days of immersion in SBF and further confirmed from XRD pattern The antibacterial study of forsterite doped nanocomposite showed good antibacterial activity against *S. aureus* and *E. coli*	60
8	Forsterite powders were prepared by sol–gel combustion method using glycine (FG) and urea (FU) as fuels	Forsterite scaffold (FG) showed higher compressive strength (201 MPa) and Young's modulus (4.8 GPa) compared to FU showed compressive strength (124 MPa) and Young's modulus (4.6 GPa)	The forsterite prepared using glycine as fuel showed higher degradation rate (2.8%) compared to forsterite prepared using urea (0.78%) after 30 days	45
9	Pure forsterite and self-curing nano forsterite biocomposites (2,2-(bis-GMA and TEGDMA) were prepared by sol–gel method.	The compressive strength, flexural strength, and diametral tensile strength was found to be increased with 50 wt% addition of forsterite in organic phase whereas the compressive modulus and flexural modulus increased upon addition of 70 wt% forsterite	AFM and XPS proved that addition of forsterite (5–70 wt%) induced the formation of HA after 28 days of immersion in SBF Complete coverage of viable well attached Saos-2 cells was seen on the surface of nano forsterite (5–70 wt%) samples	62
10	Nano forsterite powder was synthesized by sol–gel process	–	After 14 days of immersion tiny ball like apatite was seen on the surface of nano forsterite powder. EDX confirms the presence of Ca and P peaks. XRD showed characteristic peak of apatite. FT-IR showed apatite peaks at 471 cm^{-1}, 574 cm^{-1}, 1030–1090 cm^{-1}	41
11	Forsterite and mesoporous forsterite was prepared by sol–gel method	–	Needle shaped apatite crystals were seen on the surface of mesoporous forsterite samples after immersion for 7 days in SBF. EDX confirmed the Ca and P peaks in addition to Mg and Si. The optical density (OD) values of MC3T3-E1 cells on mesoporous forsterite was found to be increased compared to non mesoporous and TCP samples at 7 days. The ALP activity of mesoporous forsterite exhibited enhanced proliferation of MC3T3-E1 cells compared to control at 7 days	65
12	The ordered mesoporous forsterite (OMMS) was synthesized by sol–gel method	–	The MTT assay of ordered mesoporous magnesium silicate with varying the calcination temperature showed no toxic effect confirming the biocompatibility of all the samples	66
13	Forsterite powders were prepared by sol–gel method	The bending strength and fracture toughness of forsterite compacts was found to be 203 Mpa and 2.4 Mpa $m^{1/2}$ respectively	The MTT assay exhibited significant osteoblast proliferation rate on forsterite ceramics compared to control after 7 days	19

Table 4 continued

S. no	Preparatory methods	Mechanical properties	Biological properties	References
14	Undoped and Sr-doped (1, 2 and 3 wt%) forsterite bioceramics were prepared by solid-state method	–	With increase in time and dopant concentration from 0 to 3 wt% Sr in forsterite the degradation rate of the ceramics significantly increased The in vitro cytocompatibility of all the forsterite ceramics showed improved proliferation and differentiation of MC3T3-E1 cells The 3D micro-CT and SEM showed enhanced in vivo bone regeneration for undoped and Sr-doped samples after 30 and 90 days of implantation in rabbit model. Further the quantitative analysis of new regeneration by oxytetracycline fluorochrome labelling showed 80 ± 2% of new bone formation for 2 wt% Sr-doped forsterite samples compared to pure forsterite (42 ± 2%) The histological analysis of heart, kidney and liver after 90 days of post-implantation showed no major degenerative changes in vital organs	10
15	Forsterite nanopowder was synthesized by a combination of sol–gel and ball milling methods	–	The in vitro bioactivity of the forsterite samples showed tiny small particles (10 μm) of apatite on the surface after immersion in SBF for 21 days. EDX confirmed the particles to be Ca and P. FT-IR showed the hydroxyl groups at 3500 and 1621 cm^{-1} and around 1462 and 1420 cm^{-1} to be carbonate groups of apatite	52
16	Pure forsterite nanopowders were synthesized by an ultrafast, green synthesis via microwave irradiation method	–	SEM micrographs of forsterite samples after immersion for 14 and 21 days showed cauliflower-like structure completely covering the samples. Further, EDX confirmed the precipitated surface to be Ca and P elements The cell proliferation and viability of MG63 cells on the forsterite samples showed a significant enhancement after 3 and 5 days compared to TCP as control confirming no inhibitory effect	55
17	The nanostructured forsterite powders were prepared by two-step sintering of sol–gel method	The hardness and fracture toughness of nano forsterite ceramics were found to be 1102 Hv and 4.3 MPa $m^{1/2}$ respectively	The dissoluted products of forsterite significantly promoted G292 cell adhesion and proliferation on the surface of nanostructure forsterite ceramics	71
18	Forsterite scaffold was fabricated by sol–gel combustion method using urea as fuel	The compressive strength of forsterite scaffold prepared using urea as fuel showed 27.18 ± 13.4 MPa	Forsterite scaffold exhibited good cell attachment and proliferation of human bone marrow-derived mesenchymal cells (hBMSCs). Further, it significantly induced the osteogenic differentiation at day 14 compared to commercial bone substitute	74

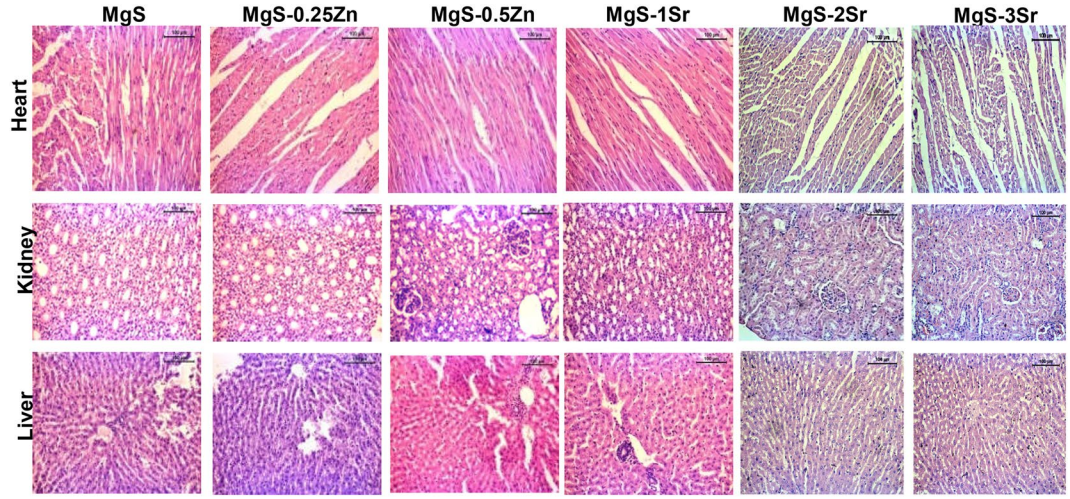

Fig. 19 Histological analysis of toxicity of forsterite. **a** Heart, **b** kidney, **c** liver after 90 days of implantation using H&E staining (scale bar = 100 μm), from Devi et al.[10, 46]

for bone tissue applications has been promoted. However, complete understanding of forsterite for orthopaedic application is still in a young stage. Several studies have reported that the degraded Mg and Si ions showed a positive effect on in vitro studies. In spite of promising aspects, there is a knowledge gap of detailed in vivo studies and clinical trials. In-depth research is needed in understanding the mechanism how various parameters influence the healing process, replacing the material with the new bone. The presence of porosity in the material plays an essential role in the choice of bone formation. Therefore, it is very important to study the nature and size of pore which helps in quality and quantity of bone formation.

The current research has been focussed on the development of materials which support osteogenesis and angiogenesis. Because of the advanced technologies in the synthesis methods, the implant materials can be tuned up with the desired porosity and other essential properties that support bone regeneration. The natural bone does not have uniform pore distribution and porosity throughout. Therefore, it is not an essential property of the implant to be uniformly porous with desired pore size and porosity. The distribution of interconnected porous structure can be tailored through manufacturing techniques that will govern both the mechanical strength and interconnected porous structure. Significant studies have been carried on calcium phosphate- and silicate-based ceramics. However, these ceramics do not satisfy the requirements of an ideal implant, mainly as a degradable material. Studies have showed that magnesium-based silicate ceramics had excellent mechanical properties with good cytocompatibility. Nano form of forsterite was highly bioactive with enhanced degradation rate, suggesting the tunable in vitro and in vivo biocompatibility. Further, combining these magnesium-based silicate ceramics with biopolymers and drugs will create a promising path to explore. This review shows that magnesium-based silicate bioceramics are promising materials for the development of various orthopaedic implant applications.

Publisher's Note

Acknowledgements

M.R. would like to acknowledge the financial assistance from Science and Engineering Research Board (SERB-SB/FTP/ETA-0114/2014), Department of Science and Technology (DST), India. S.K.N. would like to acknowledge the support from the Honourable Vice Chancellor, West Bengal University of Animal and Fishery Sciences, Kolkata.

Received: 30 May 2019 Accepted: 20 August 2019
Published online: 3 September 2019

References

1. Saini M, Singh Y, Arora P, Arora V, Jain K (2015) Implant biomaterials: a comprehensive review. World J Clin Cases WJCC 3(1):52–57. https://doi.org/10.12998/wjcc.v3.i1.52

2. Liu X, Ma PX (2004) Polymeric scaffolds for bone tissue engineering. Ann Biomed Eng 32(3):477–486
3. Nabiyouni M, Brückner T, Zhou H, Gbureck U, Bhaduri SB (2018) Magnesium-based bioceramics in orthopedic applications. Acta Biomater 66:23–43. https://doi.org/10.1016/j.actbio.2017.11.033
4. Lutton P, Ben-Nissan B (1997) The status of biomaterials for orthopedic and dental applications: part II—bioceramics in orthopedic and dental applications. Mater Technol 12(3–4):107–111. https://doi.org/10.1080/10667857.1997.11752739
5. Saad M, Akhtar S, Srivastava S (2018) Composite polymer in orthopedic implants: a review. Mater Today Proc 5(9, Part 3):20224–20231. https://doi.org/10.1016/j.matpr.2018.06.393
6. Prakasam M, Locs J, Salma-Ancane K, Loca D, Largeteau A, Berzina-Cimdina L (2017) Biodegradable materials and metallic implants—a review. J Funct Biomater. https://doi.org/10.3390/jfb8040044
7. Vallet-Regí M, González-Calbet JM (2004) Calcium phosphates as substitution of bone tissues. Prog Solid State Chem 32(1):1–31. https://doi.org/10.1016/j.progsolidstchem.2004.07.001
8. Hofmann MP, Mohammed AR, Perrie Y, Gbureck U, Barralet JE (2009) High-strength resorbable brushite bone cement with controlled drug-releasing capabilities. Acta Biomater 5(1):43–49. https://doi.org/10.1016/j.actbio.2008.08.005
9. Apelt D, Theiss F, El-Warrak AO, Zlinszky K, Bettschart-Wolfisberger R, Bohner M, Matter S, Auer JA, von Rechenberg B (2004) In vivo behavior of three different injectable hydraulic calcium phosphate cements. Biomaterials 25(7–8):1439–1451
10. Devi KB, Tripathy B, Roy A, Lee B, Kumta PN, Nandi SK, Roy M (2019) In vitro biodegradation and in vivo biocompatibility of forsterite bio-ceramics: effects of strontium substitution. ACS Biomater Sci Eng 5(2):530–543. https://doi.org/10.1021/acsbiomaterials.8b00788
11. Sheikh Z, Najeeb S, Khurshid Z, Verma V, Rashid H, Glogauer M (2015) Biodegradable materials for bone repair and tissue engineering applications. Materials 8(9):5744–5794. https://doi.org/10.3390/ma8095273
12. Yusop AH, Bakir AA, Shaharom NA, Abdul Kadir MR, Hermawan H (2019) Porous biodegradable metals for hard tissue scaffolds: a review. https://www.hindawi.com/journals/ijbm/2012/641430/. Accessed 16 Apr 2019. https://doi.org/10.1155/2012/641430
13. Yazdimamaghani M, Razavi M, Vashaee D, Moharamzadeh K, Boccaccini AR, Tayebi L (2017) Porous magnesium-based scaffolds for tissue engineering. Mater Sci Eng C 71:1253–1266. https://doi.org/10.1016/j.msec.2016.11.027
14. Diba M, Fathi MH, Kharaziha M (2011) Novel forsterite/polycaprolactone nanocomposite scaffold for tissue engineering applications. Mater Lett 65(12):1931–1934. https://doi.org/10.1016/j.matlet.2011.03.047
15. Rude RK, Gruber HE, Norton HJ, Wei LY, Frausto A, Kilburn J (2006) Reduction of dietary magnesium by only 50% in the rat disrupts bone and mineral metabolism. Osteoporos Int J Establ Result Coop Eur Found Osteoporos Natl Osteoporos Found USA 17(7):1022–1032. https://doi.org/10.1007/s00198-006-0104-3
16. Li H, Xue K, Kong N, Liu K, Chang J (2014) Silicate bioceramics enhanced vascularization and osteogenesis through stimulating interactions between endothelia cells and bone marrow stromal cells. Biomaterials 35(12):3803–3818. https://doi.org/10.1016/j.biomaterials.2014.01.039
17. Devi KB, Lee B, Roy A, Kumta PN, Roy M (2017) Effect of zinc oxide doping on in vitro degradation of magnesium silicate bioceramics. Mater Lett 207:100–103. https://doi.org/10.1016/j.matlet.2017.07.052
18. Naghiu MA, Gorea M, Mutch E, Kristaly F, Tomoaia-Cotisel M (2013) Forsterite nanopowder: structural characterization and biocompatibility evaluation. J Mater Sci Technol 29(7):628–632. https://doi.org/10.1016/j.jmst.2013.04.007
19. Ni S, Chou L, Chang J (2007) Preparation and characterization of forsterite (Mg_2SiO_4) bioceramics. Ceram Int 33(1):83–88. https://doi.org/10.1016/j.ceramint.2005.07.021
20. Wolf FI, Cittadini A (2003) Chemistry and biochemistry of magnesium. Mol Aspects Med 24(1–3):3–9
21. Weisinger JR, Bellorín-Font E (1998) Magnesium and phosphorus. Lancet Lond Engl 352(9125):391–396. https://doi.org/10.1016/S0140-6736(97)10535-9
22. Huang Y, Jin X, Zhang X, Sun H, Tu J, Tang T, Chang J, Dai K (2009) In vitro and in vivo evaluation of akermanite bioceramics for bone regeneration. Biomaterials 30(28):5041–5048. https://doi.org/10.1016/j.biomaterials.2009.05.077
23. Yoshizawa S, Brown A, Barchowsky A, Sfeir C (2014) Magnesium ion stimulation of bone marrow stromal cells enhances osteogenic activity, simulating the effect of magnesium alloy degradation. Acta Biomater 10(6):2834–2842. https://doi.org/10.1016/j.actbio.2014.02.002
24. Gu H, Guo F, Zhou X, Gong L, Zhang Y, Zhai W, Chen L, Cen L, Yin S, Chang J et al (2011) The stimulation of osteogenic differentiation of human adipose-derived stem cells by ionic products from akermanite dissolution via activation of the ERK pathway. Biomaterials 32(29):7023–7033. https://doi.org/10.1016/j.biomaterials.2011.06.003
25. A novel open-porous magnesium scaffold with controllable microstructures and properties for bone regeneration. https://www.ncbi.nlm.nih.gov/pmc/articles/PMC4829853/. Accessed 20 Apr 2019
26. Rude RK, Gruber HE, Wei LY, Frausto A, Mills BG (2003) Magnesium deficiency: effect on bone and mineral metabolism in the mouse. Calcif Tissue Int 72(1):32–41. https://doi.org/10.1007/s00223-001-1091-1

27. Rude RK, Gruber HE, Norton HJ, Wei LY, Frausto A, Kilburn J (2005) Dietary magnesium reduction to 25% of nutrient requirement disrupts bone and mineral metabolism in the rat. Bone 37(2):211–219. https://doi.org/10.1016/j.bone.2005.04.005
28. Rude RK, Kirchen ME, Gruber HE, Stasky AA, Meyer MH (1998) Magnesium deficiency induces bone loss in the rat. Miner Electrolyte Metab 24(5):314–320
29. Rude RK, Singer FR, Gruber HE (2009) Skeletal and hormonal effects of magnesium deficiency. J Am Coll Nutr 28(2):131–141
30. Khan AF, Saleem M, Afzal A, Ali A, Khan A, Khan AR (2014) Bioactive behavior of silicon substituted calcium phosphate based bioceramics for bone regeneration. Mater Sci Eng C 35:245–252. https://doi.org/10.1016/j.msec.2013.11.013
31. Szurkowska K, Kolmas J (2017) Hydroxyapatites enriched in silicon—bioceramic materials for biomedical and pharmaceutical applications. Prog Nat Sci Mater Int 27(4):401–409. https://doi.org/10.1016/j.pnsc.2017.08.009
32. Jurkić LM, Cepanec I, Pavelić SK, Pavelić K (2013) Biological and therapeutic effects of ortho-silicic acid and some ortho-silicic acid-releasing compounds: new perspectives for therapy. Nutr Metab 10:2. https://doi.org/10.1186/1743-7075-10-2
33. Zou S, Ireland D, Brooks RA, Rushton N, Best S (2009) The effects of silicate ions on human osteoblast adhesion, proliferation, and differentiation. J Biomed Mater Res B Appl Biomater 90(1):123–130. https://doi.org/10.1002/jbm.b.31262
34. Balamurugan A, Rebelo AHS, Lemos AF, Rocha JHG, Ventura JMG, Ferreira JMF (2008) Suitability evaluation of sol–gel derived si-substituted hydroxyapatite for dental and maxillofacial applications through in vitro osteoblasts response. Dent Mater Off Publ Acad Dent Mater 24(10):1374–1380. https://doi.org/10.1016/j.dental.2008.02.017
35. Aminian A, Solati-Hashjin M, Samadikuchaksaraei A, Bakhshi F, Gorjipour F, Farzadi A, Moztarzadeh F, Schmücker M (2011) Synthesis of silicon-substituted hydroxyapatite by a hydrothermal method with two different phosphorous sources. Ceram Int 37(4):1219–1229. https://doi.org/10.1016/j.ceramint.2010.11.044
36. Patel N, Best SM, Bonfield W, Gibson IR, Hing KA, Damien E, Revell PA (2002) A comparative study on the in vivo behavior of hydroxyapatite and silicon substituted hydroxyapatite granules. J Mater Sci Mater Med 13(12):1199–1206. https://doi.org/10.1023/A:1021114710076
37. In vivo assessment of hydroxyapatite and silicate-substituted hydroxyapatite granules using an ovine defect model | SpringerLink https://link.springer.com/article/10.1007%2Fs10856-005-6983-6. Accessed 20 Apr 2019
38. Tavangarian F, Emadi R (2009) Mechanical activation assisted synthesis of pure nanocrystalline forsterite powder. J Alloys Compd 485(1):648–652. https://doi.org/10.1016/j.jallcom.2009.06.051
39. Fathi MH, Kharaziha M (2008) Mechanically activated crystallization of phase pure nanocrystalline forsterite powders. Mater Lett 62(27):4306–4309. https://doi.org/10.1016/j.matlet.2008.07.015
40. Tavangarian F, Emadi R (2010) Synthesis of pure nanocrystalline magnesium silicate powder. Ceram Silik 54(2):122–127
41. Kharaziha M, Fathi MH (2009) Synthesis and characterization of bioactive forsterite nanopowder. Ceram Int 35(6):2449–2454. https://doi.org/10.1016/j.ceramint.2009.02.001
42. Sanosh KP, Balakrishnan A, Francis L, Kim TN (2010) Sol–gel synthesis of forsterite nanopowders with narrow particle size distribution. J Alloys Compd 495(1):113–115. https://doi.org/10.1016/j.jallcom.2010.01.097
43. Jones SA, Wong S, Burlitch JM, Viswanathan S, Kohlstedt DL (1997) Sol–gel synthesis and characterization of magnesium silicate thin films. Chem Mater 9(11):2567–2576. https://doi.org/10.1021/cm970401m
44. Li Q, Zhang J, Lu Q, Lu J, Li J, Dong C, Zhu Q (2016) Hydrothermal synthesis and characterization of ordered mesoporous magnesium silicate-silica for dyes adsorption. Mater Lett 170:167–170. https://doi.org/10.1016/j.matlet.2016.02.029
45. Choudhary R, Chatterjee A, Venkatraman SK, Koppala S, Abraham J, Swamiappan S (2018) Antibacterial forsterite (Mg_2SiO_4) scaffold: a promising bioceramic for load bearing applications. Bioact Mater 3(3):218–224. https://doi.org/10.1016/j.bioactmat.2018.03.003
46. Devi KB, Tripathy B, Kumta PN, Nandi SK, Roy M (2018) In vivo biocompatibility of zinc-doped magnesium silicate bio-ceramics. ACS Biomater Sci Eng 4(6):2126–2133. https://doi.org/10.1021/acsbiomaterials.8b00297
47. Ramesh S, Yaghoubi A, Sara Lee KY, Christopher Chin KM, Purbolaksono J, Hamdi M, Hassan MA (2013) Nanocrystalline forsterite for biomedical applications: synthesis, microstructure and mechanical properties. J Mech Behav Biomed Mater 25:63–69. https://doi.org/10.1016/j.jmbbm.2013.05.008
48. Anovitz LM, Rondinone AJ, Sochalski-Kolbus L, Rosenqvist J, Cheshire MC (2017) Nano-scale synthesis of the complex silicate minerals forsterite and enstatite. J Colloid Interface Sci 495:94–101. https://doi.org/10.1016/j.jcis.2017.01.052
49. Tavangarian F, Emadi R (2011) Nanostructure effects on the bioactivity of forsterite bioceramic. Mater Lett 65(4):740–743. https://doi.org/10.1016/j.matlet.2010.11.014
50. Saberi A, Alinejad B, Negahdari Z, Kazemi F, Almasi A (2007) A novel method to low temperature synthesis of nanocrystalline forsterite. Mater Res Bull 42(4):666–673. https://doi.org/10.1016/j.materresbull.2006.07.020
51. Tavangarian F, Emadi R (2010) Synthesis of nanocrystalline forsterite (Mg_2SiO_4) powder by combined

mechanical activation and thermal treatment. Mater Res Bull 45(4):388–391. https://doi.org/10.1016/j.materresbull.2009.12.032

52. Mirhadi SM, Forghani A, Tavangarian F (2016) A modified method to synthesize single-phase forsterite nanoparticles at low temperature. Ceram Int 42(7):7974–7979. https://doi.org/10.1016/j.ceramint.2016.01.195
53. Tavangarian F, Emadi R, Shafyei A (2010) Influence of mechanical activation and thermal treatment time on nanoparticle forsterite formation mechanism. Powder Technol 198(3):412–416. https://doi.org/10.1016/j.powtec.2009.12.007
54. Barzegar Bafrooei H, Ebadzadeh T, Majidian H (2014) Microwave synthesis and sintering of forsterite nanopowder produced by high energy ball milling. Ceram Int 40(2):2869–2876. https://doi.org/10.1016/j.ceramint.2013.10.025
55. Kheradmandfard M, Kashani-Bozorg SF, Noori-Alfesharaki AH, Kharazi AZ, Kheradmandfard M, Abutalebi N (2018) Ultra-fast, highly efficient and green synthesis of bioactive forsterite nanopowder via microwave irradiation. Mater Sci Eng C 92:236–244. https://doi.org/10.1016/j.msec.2018.06.026
56. Bohner M (2009) Silicon-substituted calcium phosphates—a critical view. Biomaterials 30(32):6403–6406. https://doi.org/10.1016/j.biomaterials.2009.08.007
57. DeVoe K, Banerjee S, Roy M, Bandyopadhyay A, Bose S (2012) Resorbable tricalcium phosphates for bone tissue engineering: influence of SrO doping. J Am Ceram Soc 95(10):3095–3102. https://doi.org/10.1111/j.1551-2916.2012.05356.x
58. Bandyopadhyay A, Bernard S, Xue W, Bose S (2006) Calcium phosphate-based resorbable ceramics: influence of MgO, ZnO, and SiO_2 dopants. J Am Ceram Soc 89(9):2675–2688. https://doi.org/10.1111/j.1551-2916.2006.01207.x
59. Gheitanchi R, Kharaziha M, Emadi R (2017) Sr-doped forsterite nanopowder: synthesis and biological properties. Ceram Int 43(15):12018–12025. https://doi.org/10.1016/j.ceramint.2017.06.054
60. Saqaei M, Fathi M, Edris H, Mortazavi V, Hosseini N (2016) Effects of adding forsterite bioceramic on in vitro activity and antibacterial properties of bioactive glass-forsterite nanocomposite powders. Adv Powder Technol 27(5):1922–1932. https://doi.org/10.1016/j.apt.2016.06.023
61. Teimouri A, Ghorbanian L, Najafi Chermahini A, Emadi R (2014) Fabrication and characterization of silk/forsterite composites for tissue engineering applications. Ceram Int 40(5):6405–6411. https://doi.org/10.1016/j.ceramint.2013.12.051
62. Furtos G, Naghiu MA, Declercq H, Gorea M, Prejmerean C, Pana O, Tomoaia-Cotisel M (2016) Nano forsterite biocomposites for medical applications: mechanical properties and bioactivity. J Biomed Mater Res B Appl Biomater 104(7):1290–1301. https://doi.org/10.1002/jbm.b.33396
63. LeGeros RZ (2008) Calcium phosphate-based osteoinductive materials. Chem Rev 108(11):4742–4753. https://doi.org/10.1021/cr800427g
64. Bohner M, Loosli Y, Baroud G, Lacroix D (2011) Commentary: deciphering the link between architecture and biological response of a bone graft substitute. Acta Biomater 7(2):478–484. https://doi.org/10.1016/j.actbio.2010.08.008
65. Wu Z, Tang T, Guo H, Tang S, Niu Y, Zhang J, Zhang W, Ma R, Su J, Liu C et al (2014) In vitro degradability, bioactivity and cell responses to mesoporous magnesium silicate for the induction of bone regeneration. Colloids Surf B Biointerfaces 120:38–46. https://doi.org/10.1016/j.colsurfb.2014.04.010
66. Bigham A, Hassanzadeh-Tabrizi SA, Rafienia M, Salehi H (2016) Ordered mesoporous magnesium silicate with uniform nanochannels as a drug delivery system: the effect of calcination temperature on drug delivery rate. Ceram Int 42(15):17185–17191. https://doi.org/10.1016/j.ceramint.2016.08.009
67. Ghods B, Rezaei M, Meshkani F (2016) Synthesis of nanostructured magnesium silicate with high surface area and mesoporous structure. Ceram Int 42(6):6883–6890. https://doi.org/10.1016/j.ceramint.2016.01.073
68. Hing KA (1825) Bone repair in the twenty-first century: biology, chemistry or engineering? Philos Trans A Math Phys Eng Sci 2004(362):2821–2850. https://doi.org/10.1098/rsta.2004.1466
69. Ghomi H, Jaberzadeh M, Fathi MH (2011) Novel fabrication of forsterite scaffold with improved mechanical properties. J Alloys Compd 509(5):L63–L68. https://doi.org/10.1016/j.jallcom.2010.10.106
70. Carter DR, Hayes WC (1976) Bone compressive strength: the influence of density and strain rate. Science 194(4270):1174–1176. https://doi.org/10.1126/science.996549
71. Kharaziha M, Fathi MH (2010) Improvement of mechanical properties and biocompatibility of forsterite bioceramic addressed to bone tissue engineering materials. J Mech Behav Biomed Mater 3(7):530–537. https://doi.org/10.1016/j.jmbbm.2010.06.003
72. Kwon SY, Kim YS, Woo YK, Kim SS, Park JB (1997) Hydroxyapatite impregnated bone cement: in vitro and in vivo studies. Biomed Mater Eng 7(2):129–140
73. Vallo CI, Montemartini PE, Fanovich MA, López JMP, Cuadrado TR (1999) Polymethylmethacrylate-based bone cement modified with hydroxyapatite. J Biomed Mater Res 48(2):150–158. https://doi.org/10.1002/(SICI)1097-4636(1999)48:2%3c150:AID-JBM9%3e3.0.CO;2-D
74. Krishnamurithy G, Mohan S, Yahya NA, Mansor A, Murali MR, Raghavendran HRB, Choudhary R, Sasikumar S, Kamarul T (2019) The Physicochemical and biomechanical profile of forsterite and its osteogenic

potential of mesenchymal stromal cells. PLoS One 14(3):e0214212. https://doi.org/10.1371/journal.pone.0214212

75. Nair MB, Bernhardt A, Lode A, Heinemann C, Thieme S, Hanke T, Varma H, Gelinsky M, John A (2009) A bioactive triphasic ceramic-coated hydroxyapatite promotes proliferation and osteogenic differentiation of human bone marrow stromal cells. J Biomed Mater Res A 90(2):533–542. https://doi.org/10.1002/jbm.a.32114
76. Kim JA, Yun H-S, Choi Y-A, Kim J-E, Choi S-Y, Kwon T-G, Kim YK, Kwon T-Y, Bae MA, Kim NJ et al (2018) Magnesium phosphate ceramics incorporating a novel indene compound promote osteoblast differentiation in vitro and bone regeneration in vivo. Biomaterials 157:51–61. https://doi.org/10.1016/j.biomaterials.2017.11.032
77. Li RW, Kirkland NT, Truong J, Wang J, Smith PN, Birbilis N, Nisbet DR (2014) The influence of biodegradable magnesium alloys on the osteogenic differentiation of human mesenchymal stem cells. J Biomed Mater Res A 102(12):4346–4357. https://doi.org/10.1002/jbm.a.35111
78. Hoppe A, Güldal NS, Boccaccini AR (2011) A review of the biological response to ionic dissolution products from bioactive glasses and glass-ceramics. Biomaterials 32(11):2757–2774. https://doi.org/10.1016/j.biomaterials.2011.01.004
79. Huang M, Zhang M, Yao D, Chen X, Pu X, Liao X, Huang Z, Yin G (2017) Dissolution behavior of CaO–MgO–SiO_2-based bioceramic powders in simulated physiological environments. Ceram Int 43(13):9583–9592. https://doi.org/10.1016/j.ceramint.2017.03.130
80. Zhang M, Chen X, Pu X, Liao X, Huang Z, Yin G (2017) Dissolution behavior of CaO–MgO–SiO_2-based multiphase bioceramic powders and effects of the released ions on osteogenesis. J Biomed Mater Res A 105(11):3159–3168. https://doi.org/10.1002/jbm.a.36154
81. Choudhary R, Manohar P, Vecstaudza J, Yáñez-Gascón MJ, Sánchez HP, Nachimuthu R, Locs J, Swamiappan S (2017) Preparation of nanocrystalline forsterite by combustion of different fuels and their comparative in-vitro bioactivity, dissolution behaviour and antibacterial studies. Mater Sci Eng, C 77:811–822. https://doi.org/10.1016/j.msec.2017.03.308
82. O'Neill E, Awale G, Daneshmandi L, Umerah O, Lo KW-H (2018) The roles of ions on bone regeneration. Drug Discov Today 23(4):879–890. https://doi.org/10.1016/j.drudis.2018.01.049
83. Rude RK, Gruber HE, Norton HJ, Wei LY, Frausto A, Kilburn J (2006) Reduction of dietary magnesium by only 50% in the rat disrupts bone and mineral metabolism. Osteoporos Int J Establ Result Coop Eur Found Osteoporos Natl Osteoporos Found USA 17(7):1022–1032. https://doi.org/10.1007/s00198-006-0104-3
84. Diba M, Goudouri O-M, Tapia F, Boccaccini AR (2014) Magnesium-containing bioactive polycrystalline silicate-based ceramics and glass-ceramics for biomedical applications. Curr Opin Solid State Mater Sci 18(3):147–167. https://doi.org/10.1016/j.cossms.2014.02.004
85. Ou J, Kang Y, Huang Z, Chen X, Wu J, Xiao R, Yin G (2008) Preparation and in vitro bioactivity of novel merwinite ceramic. Biomed Mater Bristol Engl 3(1):015015. https://doi.org/10.1088/1748-6041/3/1/015015
86. Iwata NY, Lee G-H, Tokuoka Y, Kawashima N (2004) Sintering behavior and apatite formation of diopside prepared by coprecipitation process. Colloids Surf B Biointerfaces 34(4):239–245. https://doi.org/10.1016/j.colsurfb.2004.01.007
87. Chen X, Ou J, Kang Y, Huang Z, Zhu H, Yin G, Wen H (2008) Synthesis and characteristics of monticellite bioactive ceramic. J Mater Sci Mater Med 19(3):1257–1263. https://doi.org/10.1007/s10856-007-3233-0
88. Abbasi-Shahni M, Hesaraki S, Behnam-Ghader AA, Hafezi-Ardakani M (2019) Mechanical properties and in vitro bioactivity of β-tri calcium phosphate, merwinite nanocomposites. https://www.scientific.net/KEM.493-494.582. Accessed 7 May 2019. https://doi.org/10.4028/www.scientific.net/KEM.493-494.582
89. Hafezi M, Reza Talebi A, Mohsen Miresmaeili S, Sadeghian F, Fesahat F (2013) Histological analysis of bone repair in rat femur via nanostructured merwinite granules. Ceram Int 39(4):4575–4580. https://doi.org/10.1016/j.ceramint.2012.11.054
90. Yang X, Xie B, Wang L, Qin Y, Henneman ZJ, Nancollas GH (2011) Influence of magnesium ions and amino acids on the nucleation and growth of hydroxyapatite. Cryst Eng Comm 13(4):1153–1158. https://doi.org/10.1039/C0CE00470G
91. Ding H, Pan H, Xu X, Tang R (2014) Toward a detailed understanding of magnesium ions on hydroxyapatite crystallization inhibition. Cryst Growth Des 14(2):763–769. https://doi.org/10.1021/cg401619s
92. Jin X, Chang J, Zhai W, Lin K (2011) Preparation and characterization of clinoenstatite bioceramics. J Am Ceram Soc 94(1):66–70. https://doi.org/10.1111/j.1551-2916.2010.04032.x
93. Mostafavi K, Ghahari M, Baghshahi S, Arabi AM (2013) Synthesis of Mg_2SiO_4:Eu3+ by combustion method and investigating its luminescence properties. J Alloys Compd 555:62–67. https://doi.org/10.1016/j.jallcom.2012.12.022
94. Sadeghzade S, Emadi R, Tavangarian F, Naderi M (2017) Fabrication and evaluation of silica-based ceramic scaffolds for hard tissue engineering applications. Mater Sci Eng C 71:431–438. https://doi.org/10.1016/j.msec.2016.10.042
95. Liu Y, Liu P, Hu C (2018) Hydrothermally assisted synthesis of pure-phase and well-dispersed forsterite nanopowders. Ceram Int 44(18):23339–23343. https://doi.org/10.1016/j.ceramint.2018.09.120
96. Fathi MH, Kharaziha M (2009) Two-step sintering of dense, nanostructural forsterite. Mater Lett 63(17):1455–1458. https://doi.org/10.1016/j.matlet.2009.03.040

K. Bavya Devi is a material chemist. She received her M.Sc. in chemistry from the University of Madras, India, in 2008. After that, she joined the research group of Professor N. Rajendran and received her Ph.D. in 2012 for the study of nanoporous bioceramic coatings on 316L stainless steel for biomedical applications. During her Ph.D., she received eight best paper awards in several international and national conferences and she was awarded National Doctoral Fellowship (NDF) by All India Council of Technical Education, New Delhi, India. Later, she joined as a postdoctoral researcher with Professor Mangal Roy's group at the Indian Institute of Technology Kharagpur, India, in 2015. Her research interests primarily focused on the development of new degradable materials that support bone regeneration and improve human health. She prepared magnesium-based degradable bioceramics because of its fundamental role in cellular processes, human metabolism, enhanced biodegradation and excellent in vitro cell–material interactions. Several metal ion dopants were used in the bioceramics to enhance the degradation and stimulate osteoblast cells. She has published several scientific articles in national and international journals.

Dr. Samit Kumar Nandi is currently Full Professor and Head, Department of Veterinary Surgery and Radiology at West Bengal University of Animal and Fishery Sciences, Kolkata, India. He received his Ph.D. in veterinary surgery and radiology from the same university. He joined in the university in 2000 as lecturer and after serving 15 years, he became professor in 2015. Dr. Nandi's research expertise lies with in vivo animal experimentation of calcium phosphate-based scaffolds and cements, 3D printed materials, silk, metal, polymers, bioactive glass as bone graft substitute, drug delivery system in osteomyelitis, coated implants in bone tissue engineering, dental implants, acellular cartilage graft and bone marrow nucleated cells in wound healing. On the basis of his research accomplishment, Dr. Nandi has received a number of national awards, including Jawaharlal Nehru Award for outstanding Post-Graduate Agricultural Research 2007 of Indian Council of Agricultural Research, prestigious National Bioscience Award 2008 for career development, Biotech Product and process Development and Commercialization Award 2013 of Department of Biotechnology, CSIR Technology Award 2010 as a part of Award winning Team, prestigious Tata Innovation Fellowship, DBT, Government of India and "Excellence of Animal Biotechnology" from Society of Applied Biotechnology, India. He also received National Teaching Excellence Award 2016 from International Benevolent Research Foundation, Science excellence Award 2015 from Foundation for Science and Environment, Kolkata, West Bengal and Best Teacher award 2016 and 2017 from his parent university. He has completed six research projects funded by DBT, DST, Ministry of Science and Technology, Government of India and is running three other projects funded by the Department of Biotechnology. Professor Nandi has supervised/supervising over 41 master's and 10 Ph.D. students in veterinary surgery and radiology and allied subjects. His students have moved to academia and national laboratories within India. He is a prolific writer and has contributed more than 130 scientific articles to national and international journals of repute, three books, ten international book chapters and submitted seven national patents (one granted). He is a reviewer of a number of journals all over the globe. He has given several invited and contributed presentations in various national and international symposia, national institutes and laboratories. Professor Nandi is Fellow of National Academy of Agricultural Sciences, Indian Society for Veterinary Surgery, Society of Applied Biotechnology, Indian Association for the Advancement of Veterinary Research and Member of National Academy of Sciences, India and National Academy of Veterinary Sciences, India.

Dr. Mangal Roy is an assistant professor in the Department of Metallurgical and Materials Engineering at the Indian Institute of Technology Kharagpur, India. He got his Ph.D. in materials science and engineering from Washington State University, Pullman, USA. After graduating with his Ph.D., he was also an Assistant research professor and research associate at the Washington State University, Pullman campus and at the University of Pittsburgh's Department of Bioengineering. His primary research interest is in tissue engineering, specifically bone remodelling, bioceramics, biodegradable metals, and surface modification of biomaterials. He has almost 15 years of experience in tissue engineering of bone replacement materials that includes both in vitro and in vivo characterizations. He has written three book chapters and published 36 journal articles along with two conference publications. He obtained a bachelor of technology in ceramic technology from the College of Ceramic Technology at Calcutta University, India, and a master's degree in ceramic engineering from the Institute of Technology, Banaras Hindu University in India.